



RESEARCH ARTICLE

WILEY

Modulation of local field potentials and neuronal activity in primate hippocampus during saccades

Guillaume Doucet^{1,2,3,4}  | Roberto A. Gulli^{3,4,5,6}  | Benjamin W. Corrigan^{3,4} |
Lyndon R. Duong^{3,4,7} | Julio C. Martinez-Trujillo^{3,4,8,9}

¹The Ottawa Hospital Research Institute, Ottawa, Ontario, Canada

²Department of Physiology, McGill University, Montreal, Quebec, Canada

³Department of Physiology and Pharmacology, Schulich School of Medicine and Dentistry, Western University, London, Ontario, Canada

⁴Robarts Research Institute, Schulich School of Medicine and Dentistry, Western University, London, Ontario, Canada

⁵Integrated Program in Neuroscience, McGill University, Montreal, Quebec, Canada

⁶Department of Neuroscience, Columbia University, New York, New York

⁷Center for Neural Science, New York University, New York, New York

⁸Department of Psychiatry, Schulich School of Medicine and Dentistry, Western University, London, Ontario, Canada

⁹Brain and Mind Institute, Western University, London, Ontario, Canada

Correspondence

Julio C. Martinez-Trujillo, Robarts Research Institute, University of Western Ontario, 1151 Richmond Street North, Room 7239, London, Ontario N6A 5B7, Canada
Email: julio.martinez@robarts.ca

Funding information

Canadian Institutes of Health Research; Natural Sciences and Engineering Research Council of Canada; BrainsCAN through the Canada First Research Excellence Fund

Abstract

Primates use saccades to gather information about objects and their relative spatial arrangement, a process essential for visual perception and memory. It has been proposed that signals linked to saccades reset the phase of local field potential (LFP) oscillations in the hippocampus, providing a temporal window for visual signals to activate neurons in this region and influence memory formation. We investigated this issue by measuring hippocampal LFPs and spikes in two macaques performing different tasks with unconstrained eye movements. We found that LFP phase clustering (PC) in the alpha/beta (8–16 Hz) frequencies followed foveation onsets, while PC in frequencies lower than 8 Hz followed spontaneous saccades, even on a homogeneous background. Saccades to a solid grey background were not followed by increases in local neuronal firing, whereas saccades toward appearing visual stimuli were. Finally, saccade parameters correlated with LFPs phase and amplitude: saccade direction correlated with delta (≤ 4 Hz) phase, and saccade amplitude with theta (4–8 Hz) power. Our results suggest that signals linked to saccades reach the hippocampus, producing synchronization of delta/theta LFPs without a general activation of local neurons. Moreover, some visual inputs co-occurring with saccades produce LFP synchronization in the alpha/beta bands and elevated neuronal firing. Our findings support the hypothesis that saccade-related signals enact sensory input-dependent plasticity and therefore memory formation in the primate hippocampus.

KEYWORDS

hippocampal LFP, macaque monkey, phase coding, phase modulation, virtual reality

1 | INTRODUCTION

In primates, saccadic eye movements shift the fovea toward regions of interest across the visual field. In between saccades, periods of stable gaze, termed fixations, allow the integration of information about stimuli falling on the fovea. Successive saccade-fixation cycles incrementally build a detailed picture of the environment (Gottlieb, Hayhoe, Hikosaka, & Rangel, 2014; Liu, Shen, Olsen, & Ryan,

2017; Samonds, Geisler, & Priebe, 2018; Zimmermann & Lappe, 2016), enacting memory associations of foveated objects, their spatial arrangement, and context. Conversely, saccade target selection can be influenced by expectations derived from these associations (Buschman & Miller, 2007; Frank & Sabatinelli, 2017; Najemnik & Geisler, 2005; Peelen & Kastner, 2014). The exact mechanisms by which saccades influence memory formation remain a matter of debate.

The hippocampus is known to play a critical role in associative memory formation and retrieval (Buffalo, 2015; Eichenbaum, 2004; Eichenbaum & Cohen, 2014; Schiller et al., 2015; Watrous & Ekstrom, 2014). Previous studies have shown that hippocampal neuronal activity is modulated around eye movement onsets in both human and nonhuman primates (Hoffman et al., 2013; Jutras, Fries, & Buffalo, 2013; Ringo, Sobotka, Diltz, & Bunce, 1994; Sobotka & Ringo, 1997; Staudigl, Hartl, Noachtar, Doeller, & Jensen, 2017). This modulation occurs in complete darkness (Sobotka & Ringo, 1997) or during rapid eye movement sleep (Andrillon, Nir, Cirelli, Tononi, & Fried, 2015), suggesting that it has an extra-retinal origin. Moreover, the onset of sensory stimuli also modulates hippocampal activity (Fell et al., 2004; Givens, 1996; Kleen et al., 2016; Mormann et al., 2005; Tesche & Karhu, 2000). It has been further hypothesized that both sensory and motor signals reach the hippocampus and evoke neural activity in different frequencies of local field potential (LFP) oscillations (Katz, Patel, Talakoub, Hoffman, & Valiante, 2018).

Some studies have reported that saccades can “reset” the phase of LFPs in both the hippocampus (Hoffman et al., 2013; Jutras et al., 2013; Sobotka & Ringo, 1997; Staudigl et al., 2017) and visual cortical areas (Bartlett, Ovasyikia, Logothetis, & Hoffman, 2011; Burr, Morrone, & Ross, 1994; Ito, Maldonado, & Grün, 2013; Ito, Maldonado, Singer, & Grün, 2011; Rajkai et al., 2008). Responses of neurons along the visual processing pathways, from the lateral geniculate nucleus to the prefrontal cortex (PFC), are typically suppressed during saccades and enhanced following saccade landing (fixation onset) (Bartlett et al., 2011; Burr et al., 1994; Ito et al., 2011, 2013; Rajkai et al., 2008; Schroeder, Wilson, Radman, Scharfman, & Lakatos, 2010). This suppression is thought to reduce the perceived motion of the external world and to facilitate perceptual integration across saccades (Ibbotson, Crowder, Cloherty, Price, & Mustari, 2008; McFarland, Bondy, Saunders, Cumming, & Butts, 2015; Moore, Armstrong, & Fallah, 2003).

In contrast, hippocampal neuronal activity decreases prior to the initiation of a saccade, at an earlier time than would be anticipated by saccadic suppression in the visual cortex (Andrillon et al., 2015). Additionally, some neurons within the hippocampus (Sobotka & Ringo, 1997), as well as within the upstream entorhinal cortex (Killian, Potter, & Buffalo, 2015), seem to be tuned to saccade direction, suggesting that signals linked to saccade parameters may reach the hippocampus. Across species, hippocampal neurons respond to visual stimuli (Kreiman, Koch, & Fried, 2000) and encode combinations of stimulus identity, value, and spatial and temporal positions, in a task-dependent manner (Fenton et al., 2010; McKenzie et al., 2016; Morris, 2006; Muzzio, Kentros, & Kandel, 2009; Rolls & Wirth, 2018; Wirth, Baraduc, Plante, Pinede, & Duhamel, 2017). For example, a subset of primate hippocampal neurons encode gaze location in the environment across changes in viewing angle, when the view is obstructed, or in complete darkness (Feigenbaum & Rolls, 1991; Georges-François, Rolls, & Robertson, 1999; Rolls, 1999; Rolls & O'Mara, 1995; Rolls, Robertson, & Georges-françois, 1997; Rolls & Wirth, 2018). These hippocampal representations can also be

reactivated by endogenous signals (Rueckemann & Buffalo, 2017; Wirth et al., 2017) further suggesting that a variety of signals related to sensory, cognitive, motor, and/or spatial processing converge within the hippocampus.

In monkeys and humans, perisaccadic LFP modulations in the hippocampus are time-locked to the onset of eye movements (Andrillon et al., 2015; Hoffman et al., 2013) and linked with memory task performance (Jutras et al., 2013; Staudigl et al., 2017). It has been specifically proposed that the hippocampus may receive a copy of the saccade command (i.e., corollary discharge; Sommer & Wurtz, 2002), which resets the phase of the LFPs to facilitate the processing of sensory information linked to an upcoming fixation target (Meister & Buffalo, 2016). However, uncertainty remains about whether this signal is generic, common to all saccades, and related to saccadic suppression; or whether it is informative about the saccade parameters, possibly holding information about the spatial relationships between objects.

To investigate these issues, we conducted a comprehensive exploratory analysis on the relationship between primate hippocampal LFPs and saccades. We recorded eye movements and neural activity from the right hippocampus of two rhesus macaques performing three different tasks: a visually guided Cued Saccade (CS) task (Figure 1a), and two virtual navigation tasks: Foraging (FOR; Figure 1b) and Associative Memory (AM; Figure 1c). Eye movements were unconstrained and were precisely aligned with electrophysiological data (Doucet, Gulli, & Martinez-Trujillo, 2016). We found that LFP phase in the alpha/beta (8–16 Hz) band preferentially clustered following visual transients and was followed by increases in spiking activity in neurons recorded from the same electrode. On the other hand, LFP phase in the delta/theta band (<8 Hz) was clustered following saccade onsets, independent of visual stimulation. Additionally, saccades to a uniform background were not followed by neuronal firing increases. Finally, delta band (≤ 4 Hz) phase and theta band (4–8 Hz) power were modulated by saccade direction and amplitude, respectively.

2 | MATERIALS AND METHODS

2.1 | Subjects

Two healthy adult male rhesus macaques (*Macaca mulatta*) were used for this study. Animals were obtained from, and were under the care of, the McGill Comparative Medicine and Animal Resources Center. Monkey W (7 years old; 7 kg) was group housed and Monkey R (14 years old; 12 kg) was single housed, and both monkeys had access to large playpen enclosures and were trained to enter a side cage prior to testing. All handling and procedures were in accordance with the Canadian Council for Animal Care Guidelines and approved by the McGill University Animal Care Committee.

2.2 | Surgical procedures

Prior to any surgical procedures, anatomical magnetic resonance imaging (MRI) scans were taken for each animal (500 μ m isotropic

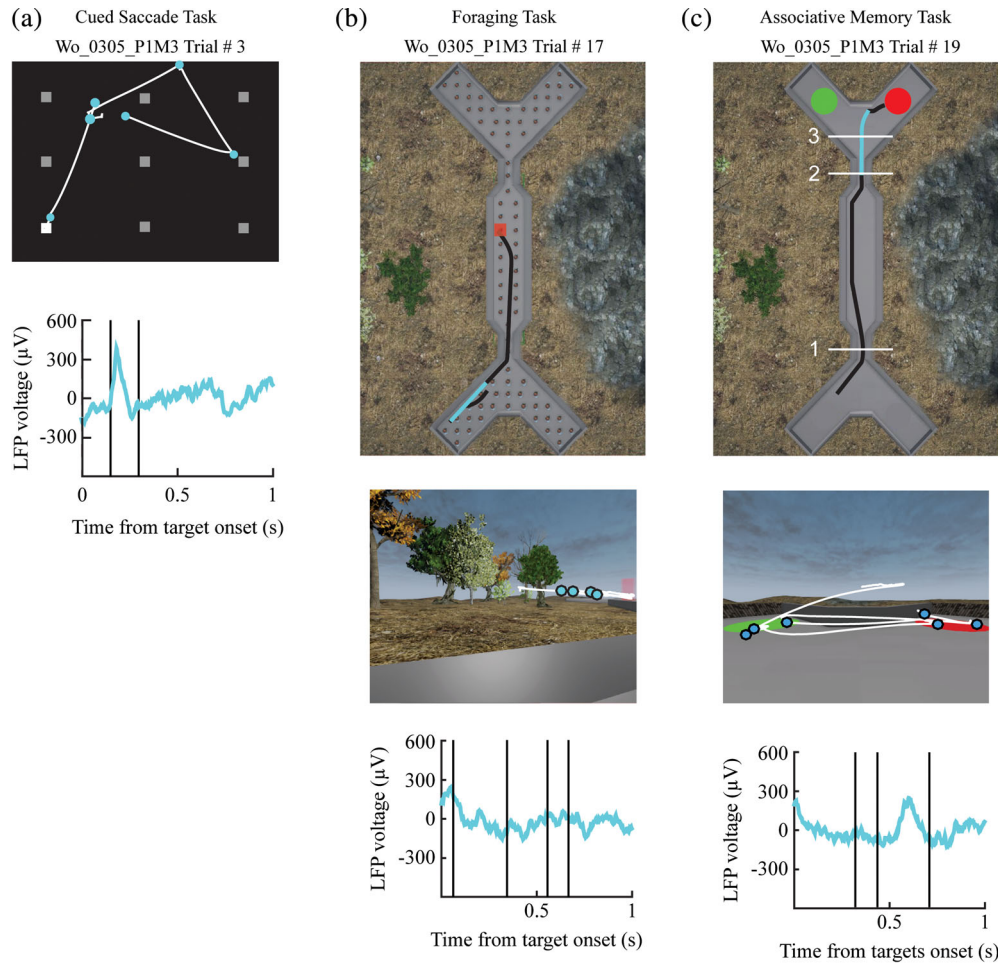


FIGURE 1 Tasks description. (a) Cued Saccade task. Monkeys were presented with a uniform grey background and freely looked until a white target appeared at one of nine possible locations (top). Target fixation was then required to obtain a juice reward. (b) Foraging task. Animals were required to navigate inside a double ended Y-maze toward a red target appearing randomly at one of 84 possible locations (top; brown dots). (c) Associative Memory task. Animals navigated back and forth along the north–south axes of the double ended Y-maze (top). Upon entering the central corridor (1) contextual information was displayed on the maze walls, (2) colored targets were displayed in both arms at the end of the corridor. The animal navigated to the target with highest reward value. Center plots show screen examples with overlaid eye traces (white) and saccade onsets (colored circles). Bottom plots display raw local field potential traces associated with the current trials; saccade onsets are marked with black bars

T1-weighted 3 Tesla field strength). We then used a neuro-navigation suite (BrainSight, Rogue Research, Quebec, Canada) to obtain a three-dimensional (3D) reconstruction of the animals' skull. Headpost and recording chamber positions were then planned and custom built from these reconstructions.

Two consecutive surgeries under general anesthesia, separated by a recovery period of at least 8 weeks, were performed to implant the headpost and subsequently the recording chamber. Recording chambers were positioned over the right prefrontal cortex, to obtain electrode trajectories perpendicular to the long and transverse axes of the right hippocampus.

Recording chamber placement was validated with a postrecovery computed tomography (CT) scan, with cannulas strategically placed within the recording chamber grid, later coregistered with the anatomical MRI scan. Electrode trajectories and terminal depths were then precisely mapped to grid holes.

2.3 | Experimental setup

Monkeys were seated in a custom-built primate chair and head-fixed ~80 cm away from a computer monitor (1,280 × 1,024 resolution; 44 × 33 cm; 32 × 24 degrees of visual angle [DVA]) refreshing at 75 Hz. The chair was also fitted with a customized two-axis joystick (M212, PQ Controls, Bristol, CT) to allow navigation in the virtual tasks. Eye movements were monitored by video-oculography (EyeLink 1,000, SR Research, Ottawa, Canada), tracking the left eye at 500 Hz.

Two separate display software were used for visual stimulation. Firstly, for the CS task, stimuli were presented using the Psychophysics Toolbox (Brainard, 1997). Secondly, the virtual navigation tasks were presented using an open-source library (Doucet et al., 2016) running a freely available videogame engine (Unreal Engine 3, Epic Games, Inc., Potomac, NC) on a separate computer. Subject positions in the virtual environment were timestamped and recorded at every

frame before being sent to the central control computer over a network link.

The central computer ran an experimental suite programmed in Matlab (Mathworks Inc., Natick, MA), tasked with temporally aligning visual stimulus, gaze, and neural data, while controlling trial progression. A juice incentive was used to reward correct trials.

2.4 | Behavioral tasks

Monkeys were trained on three separate tasks. In the CS task (Figure 1a), monkeys were simply trained to shift and hold their gaze within 2 DVA of the center of a small white dot (1 DVA diameter) pseudorandomly presented at 1 of 9 possible locations on a 24 by 16 DVA grid. The background luminance was set to match the average luminance of the virtual tasks to minimize pupil size variations.

In the FOR task (Figure 1b), monkeys were required to navigate using the two-axis joystick, inside a double-ended Y-maze, toward a semi-transparent red column randomly appearing at 1 of 84 possible locations. In the AM task (Figure 1c), monkeys navigated within the same environment as the FOR task but were required to learn a context-dependent color hierarchy. Upon entering the central corridor (Figure 1c, Point 1), one of two possible contextual cues were displayed on the maze walls. Context information dictated the order of a three-color reward hierarchy, inverted across contexts (e.g., red > green > blue in Context 1; blue > green > red in Context 2). Two randomly selected colored targets were displayed upon departure from the central corridor (Figure 1c, Point 2), one in each maze arm (Figure 1c, red and green circles). Animals then navigated toward the target with the highest reward value. Decision onset (Figure 1c, Point 3) was defined as the first point where heading differed by more than 10° from center. Learning occurred through trial and error and hierarchies were pseudorandomly selected at the start of each recording session. The two possible contexts were the same each day. The object colors changed daily.

The virtual navigation tasks did not include blank intertrial intervals, meaning that a trial began immediately as soon as the previous one ended, without breaks in visual stimulation. Only data from sessions containing at least 20 completed trials were kept for analyses (CS task: 38 sessions; FOR task: 36 sessions; AM task: 40 sessions; multinomial logistic regression [MLR] analyses: 36 sessions).

2.5 | Saccade detection

Saccades were detected using the method described in Corrigan, Gulli, Doucet, and Martinez-Trujillo (2017). Briefly, we removed blinks, off-screen gaze and periods of valid data lasting less than 40 ms, and smoothed the eye position data with a Savitzky-Golay filter (second order with an 11 samples window) prior to saccade detection. We then proceeded to identify periods of putative saccadic activity by an iteratively defined acceleration threshold: starting at 10,000 DVA/s², the sum of the mean and six times the *SD* of all acceleration values below the threshold was computed and defined as the new threshold. This procedure was repeated until the net iteration change was less than 1 DVA/s². Saccadic epochs less than 40 ms apart were further

grouped into a single epoch. Values above the threshold lasting more than 10 ms were then considered saccadic epochs, from which onset and offset points were calculated.

The aforementioned procedures were modified from a pre-existing classification algorithm tailored for humans (Larsson, Nystrom, & Stridh, 2013), using a fixed threshold, defined as six times the *SD* above median acceleration (Nyström & Holmqvist, 2010). To our knowledge, no such thresholds have been defined to account for the increase in saccade rate, velocity, and signal stability in head-restrained macaque data (Corrigan et al., 2017). We thus used a lower and iteratively defined threshold to minimize false negatives and to maintain a robust separation between saccades and smooth pursuits.

Onset and offset points were obtained from the identification of eye movement directions deviating by either more than 60° for a single sample or by more than 20° for three consecutive samples, from the saccade's main direction, specified by the average direction at peak velocity and its immediate neighbors. Points were fine-tuned by confirming that the eye velocity was lower than the greater of two measures: 30 DVA/s or one-fifth of the peak velocity. Saccade parameters (i.e., amplitude and direction) were obtained from the vector linking eye positions at onset and offset. Only saccades originating and terminating on the screen were used for all analyses. Further detail about the eye movement classification procedure, as well as example eye traces, can be found in Corrigan et al. (2017).

2.6 | Saccade probability

Saccade probability across trials was obtained by first creating saccade onset raster plots for each trial, matching the LFP sampling period of 1 ms. Each raster was then convolved with an asymmetric exponential function (1 ms growth; 20 ms decay), used in spike density function analyses, to increase the precision of onset time and match neural data (Thompson, Hanes, Bichot, & Schall, 1996). Probabilities were later averaged over all trials.

2.7 | Gaze processing

Gaze target identification in the virtual navigation tasks was undertaken by first matching every displayed frame and its associated player position in the 3D environment, with the concurrent on-screen gaze position in pixels. Knowing the subject location within the environment and both horizontal and vertical fields of views, we projected the on-screen gaze onto the farthest plane of the viewing frustum, thus translating them into 3D coordinates. We then computed the base vector components linking the position of the subject's virtual eyes in the environment and the 3D gaze coordinates. To account for the approximate size of foveal vision, we repeated this procedure for another eight gaze positions equidistant on a ~1.5 DVA radius circle centered on gaze coordinates. All visible objects in the environment being traversed by these vectors were identified as foveated objects.

As multiple objects could be included within each gaze sample, we applied a behavioral relevance hierarchy (i.e., target > contextual

information > environment), where the entire sample was classified as belonging to the category of the object with highest relevance. Saccade targets were then defined as the category of the gaze sample at the time of saccade offset.

2.8 | Electrophysiological recordings and signal preprocessing

We collected data over 41 sessions, simultaneously recording with up to four single high-impedance tungsten electrodes (0.4–1.5 M Ω ; lowering speed: 0.01 mm/s; referenced to a dura penetrating guide tube). Electrode trajectories were mapped to the MRI beforehand and expected distances to grey and white matter tracts were predicted along the descending paths, terminating at putative CA3 recording sites. Neural activity changes were monitored online to approximate transitions between white and grey matter and to validate terminal recording depths.

Neural activity was recorded at 30 kHz using a multichannel data acquisition system (128 channels Cerebus System, BlackRock Microsystems, Salt Lake City, UT) with analog 0.3 Hz and 7.5 kHz high-pass and low-pass filters. We then filtered the signal backwards with matching digital filters to correct for phase shifts induced by hardware filters (Cohen, 2014; Zanos, Mineault, & Pack, 2011). To obtain the raw LFP signal, we further low-pass filtered the data (zero-phase using Matlab function *filtfilt*; 250 Hz cutoff, fourth-order Butterworth) and removed power line noise using third-order two-pass elliptical band-stop filters at 60, 120, and 180 Hz (Zanos, Zanos, Marmarelis, Ojemann, & Fetz, 2012). LFP data were then down-sampled to 1 kHz and manually thresholded for artifact removal. All values exceeding the set threshold were discarded from future analyses.

In order to account for differences in baseline voltage and signal amplitude across electrodes, LFP voltage values (Figures 3–6) were first z-scored over their entire recording session. This procedure thus kept the shape of individual waveforms constant, while allowing for comparable scales across electrodes and conditions. Note that raw voltage values were used for power and phase computations.

Spiking neurons were isolated while animals quietly sat in the dark prior to the experiments. Artifactual threshold crossings were manually removed using Offline Sorter (Plexon Inc., Dallas, TX). Further details are available in Gulli et al. (2018). To highlight global changes in neuronal activity around saccade and stimulus onsets, a single multiunit cluster was created per electrode by pooling all threshold crossings. Spike times were then binned (1 ms step) and convolved with the same exponential kernel as the saccade probability plots (Thompson et al., 1996) to generate spike density function plots. Resulting firing rates were then z-score normalized over all events within an electrode, using a –500 to –200 ms preonset baseline.

2.9 | Power and phase computation

To obtain the analytical signal from the preprocessed LFP data, we convolved it with 34 logarithmically spaced complex Morlet wavelets, with seven oscillations (Tallon-Baudry, Bertrand, Delpuech, & Pernier,

1997) and center frequencies ranging from 2.63 to 256 Hz (Hughes, Whitten, Caplan, & Dickson, 2012; Liebe, Hoerzer, Logothetis, & Rainer, 2012; Tremblay, Doucet, Pieper, Sachs, & Martinez-Trujillo, 2015). Power was obtained from the squared magnitude of the analytical signal, while phase was derived from the angle between the real and complex parts. We avoided edge effects and allowed analyses periods to be shorter than full oscillation cycles by applying the convolution to entire recording sessions. We could therefore obtain reliable instantaneous power and phase estimations at every time point (1 ms resolution), regardless of the duration of our epochs of interest.

To account for the 1/frequency power scaling and to allow for cross-task and cross-electrode comparisons, we z-scored the power values, for each center frequency individually, within entire recording sessions, regardless of behavior.

2.10 | Phase clustering

To quantify the degree of phase clustering (PC) for stimulus and saccade-triggered data, we computed a PC index. This index is obtained by converting each angular phase value to a two-dimensional unit vector, and computing the norm of the average vector, resulting in an index that ranges from 0, for a uniform distribution, to 1, for identical angles (Cohen, 2014). This calculation was completed independently within each electrode for all time–frequency points (1 ms sampling period) in a 2-s window for intertrial PC ($\pm 1,000$ ms; Figure 2) and in a 1-s window for intersaccade PC (± 500 ms; Figures 3 and 4).

Moreover, as the index value is dependent on the number of points used for its computation, it is possible to estimate a theoretical significance threshold from a desired p value (Figure S3b, right):

$$PC_{\text{Threshold}} = \sqrt{\frac{-\ln(p)}{N}},$$

where N is the number of observations and p is the desired p value (Cohen, 2014), in our case set at 0.01/34 frequencies/14 bins.

2.11 | PC differences between conditions

To compare the magnitude of PC triggered by neighboring events (Figure 3, ΔPC), we measured the peak PC value for each frequency within the first 200 ms following event onset. This analysis assumes that one of the events is driving the PC (i.e., maximal value), while trial to trial variability in the interevent durations would decrease the phase coherence when aligned to nondriving events. Statistical significance between conditions was obtained by a Bonferroni corrected paired t test ($p < .05/34$ frequencies).

To avoid possible effects of inattention across conditions, only eye movements where the gaze was on the screen, from onset to offset, were kept for analyses.

2.12 | Nonparametric permutation testing

As previously stated, PC values are dependent on the number of points used for their computation, preventing the pooling of recording sessions to run group statistics. We thus computed saccade-triggered power and PC statistical significance individually for each electrode. To do so, we first created null distributions of saccade-triggered LFP power and phase by randomly shifting saccade times within each trial epoch. Of note, as rewarded targets were only visible for short durations during the CS and AM tasks, as opposed to entire trials in the FOR task, null distributions for saccade to targets in Figure 4 (CS task) were computed by shifting the saccade times within the target epoch only, and not over entire trial times. Correspondingly and to avoid the confounding effects of visual stimulation, null distributions for the background condition of the CS task (Figure 4) were obtained for the trial epochs when no targets were visible.

From the computed null distributions, average power and PC were computed, and only the maximal and minimal values for each wavelet center frequency were kept. This procedure was repeated 1,000 times to obtain frequency specific distributions of extreme values. The statistical threshold for PC values was defined as the 99th percentile of the maximal values (one-tailed), while power thresholds were defined as the 0.5th and the 99.5th percentile of the minimal and maximal value distributions (two-tailed). This method was adapted from the nonparametric permutation “pixel-based” correction method (Cohen, 2014) to account for largely different power and PC distributions across frequencies.

2.13 | Cross-electrode statistical significance and comparison

As statistical significance was computed on a per electrode basis, we devised a way to highlight time–frequency points that were consistently significant across electrodes. This is termed the significance probability. For illustration, we outlined the points where the significance probability across all channels was >5% (thin line), > 50% (middle line), or >75% of channels were significant (Figures 3 and 4, black outlines).

Moreover, to compare significance proportions across non-matched conditions, namely Figure 4, we found the peak significance probability, within the first 200 ms of each frequency band, following saccade onset and ran a chi-square test for equality of proportions across conditions. The same procedure was also undertaken to compare power across conditions. As wavelet convolution induces spectral leakage across frequency bands (i.e., they are not independent), a Bonferroni correction was applied on the p values ($p < .05/34$ frequencies).

2.14 | Multinomial logistic regression

To quantify the relationship between LFPs and saccade parameters, we needed a regression model that could fit linear (i.e., LFP power) and circular (i.e., LFP phase) independent variables to either a linear

(i.e., saccade amplitude) or a circular (i.e., saccade direction) dependent variable. To our knowledge, no regression model interchangeably accepts linear and circular data as the dependent variable. We circumvented this problem by binning saccade directions and amplitudes into, respectively, 16 (22.5°) and 14 (2 DVA) consecutive bins and regressed bin numbers by means of MLR for ordinal responses (Matlab function *mnrfit*), also identified as proportional-odds model (McCullagh, 2005). This model computes how a unit change in an independent variable affects the odds of the dependent variable being less than or equal to bins 1 to n versus bins $n + 1$ to k , where k is the total number of bins. Calculations are made for all bin numbers n , keeping all other independent variables constant. For example, Figure S3a shows that a unit changes in gamma power at time 0 significantly predicts the probability that a saccade's amplitude belongs to bins $\leq N$ versus bins $> N$.

As MLR is a generalized linear model, it assumes discrete or continuous independent variables, not circular ones. However, LFP phase values are periodic over 2π and can be expressed as a first-order Fourier series expansion (Lund, 1999; Sarma & Jammalamadaka, 1993), yielding the following regression representation:

$$\text{Bin number (Y)} \sim \beta_1 \times \text{LFP power} + \beta_2 \times \sin(\text{LFP phase}) + \beta_3 \times \cos(\text{LFP phase}) + \beta_Y,$$

where Y is the bin number and where β_Y is the bin specific intercept. The MLR model provides a single parameter for each independent variable, with a bin specific intercept value.

Although individual p values are obtained for each independent variable following model fitting, we set out to quantify the influence of both sine and cosine terms simultaneously. Parameter significance was thus computed by comparing nested models' deviance using a chi-square test, with degrees of freedom defined as the difference in the number of model parameters. For example, p value for the LFP power parameter β_1 would be calculated as 1 – the chi-square cumulative distribution function of the deviance differences between the nested model, excluding the power term and the full model. In this case, the degrees of freedom would be defined as 1 (i.e., removing β_1).

Probability values for regression parameters were computed around saccade onset by taking the instantaneous power and phase values at 17 time points from 200 ms before onset, to 200 ms after onset, in 25 ms steps. Bonferroni correction was applied to the resulting p values to determine significance ($p < .05/34$ frequencies/17 time points).

2.15 | Surrogate signal generation

We controlled for the effect of saccade amplitude on phase signal-to-noise ratio (SNR) by creating a surrogate signal with constant phase information and varying SNR. We first determined the real signal's SNR value (Figure S3d) for each amplitude bin, by applying a spike metric defined as the peak to trough amplitude of the mean LFP deflection divided by twice the SD of all deflection differences from

the mean (Kelly et al., 2007; Zanos et al., 2012). We then determined our “gold standard” waveform (i.e., constant phase) as the average saccade-triggered LFP from amplitude bins 4 to 9, identified as the most reliable (>95% significant electrodes; Figure S3b, right red outline). A “clean” background LFP signal was next generated by going through each saccade and subtracting its amplitude bin averaged LFP deflection from the raw LFP signal. Surrogate signals were thus obtained by scaling the gold standard deflection and adding it to randomly selected background LFP snippets. To properly identify scale parameters and match real data SNR (Figure S3d), we quantified the influence of a wide selection of arbitrarily selected scale values on obtained SNR via linear regression. Final scale parameters were computed by fitting real signal SNR values into our model. We limited this analysis to amplitude bins 1 to 9 (i.e., ≤ 18 DVA) as proportions of significance decreased for larger saccades due to their limited number (Figure S3c). Lack of significant differences between the real and surrogate SNR distributions was obtained from a Wilcoxon rank-sum test ($p > .05$).

3 | RESULTS

We investigated the relative contributions of target and saccade onsets to hippocampal LFPs by first examining whether saccade

frequency (Figures 2a–c, top row), LFP power (middle row) and LFP PC (bottom row) were modulated around target onsets. Note that we use the term LFP PC, rather than phase reset, to refer to oscillations that show a degree of synchrony in relationship to an event (e.g., target or saccade onset). In other words, no assumptions were made regarding the presence (i.e., phase reset) or absence (i.e., evoked response) of pre-event oscillations. Comparisons of pre- and post-target onset values, within a 500-ms window, revealed a significant increase in low-to-mid-gamma band power (~ 30 – 120 Hz) across all conditions (Figure 2d, left; paired t test, $p < .05$ Bonferroni corrected). For frequencies below 32 Hz, there was a task-dependent effect. Target onset during the CS task elicited a robust power increase across all frequencies below 12 Hz. In the FOR task, power decreased for frequencies in the beta band (~ 12 – 30 Hz). Power in the AM task was significantly decreased across most low frequencies (4–20 Hz).

PC following stimulus onset was significantly greater than pre-onset for frequencies below 12 Hz in all tasks (Figure 2d, right; paired t test, $p < .05$ Bonferroni corrected). Of note, the frequency of peak PC differences varied across tasks, from <4 Hz in the AM task to ~ 7 Hz in the CS task and to ~ 9 Hz in the FOR task. Moreover, the magnitude of PC differences seemed to correlate with the magnitude of peak saccade probabilities (Figures 2a–c, top row), where $CS > AM > FOR$. Thus, PC around target onsets seemed to be

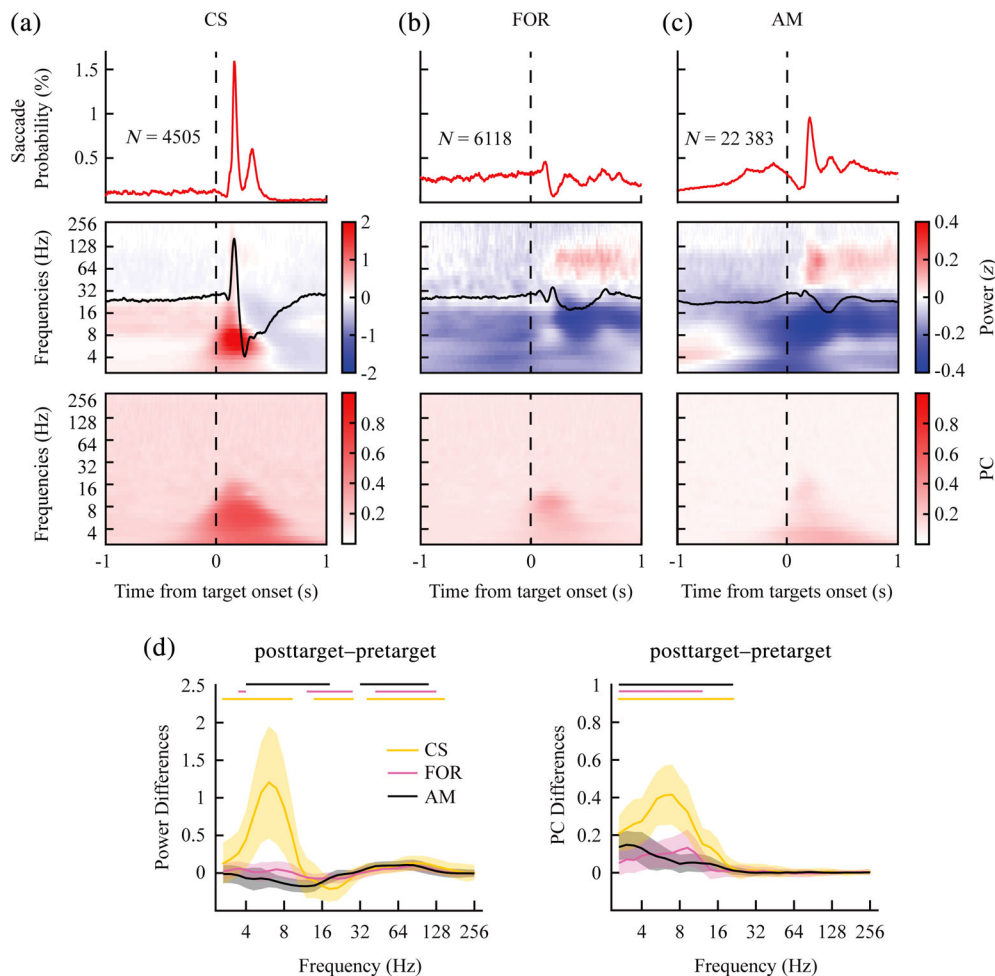
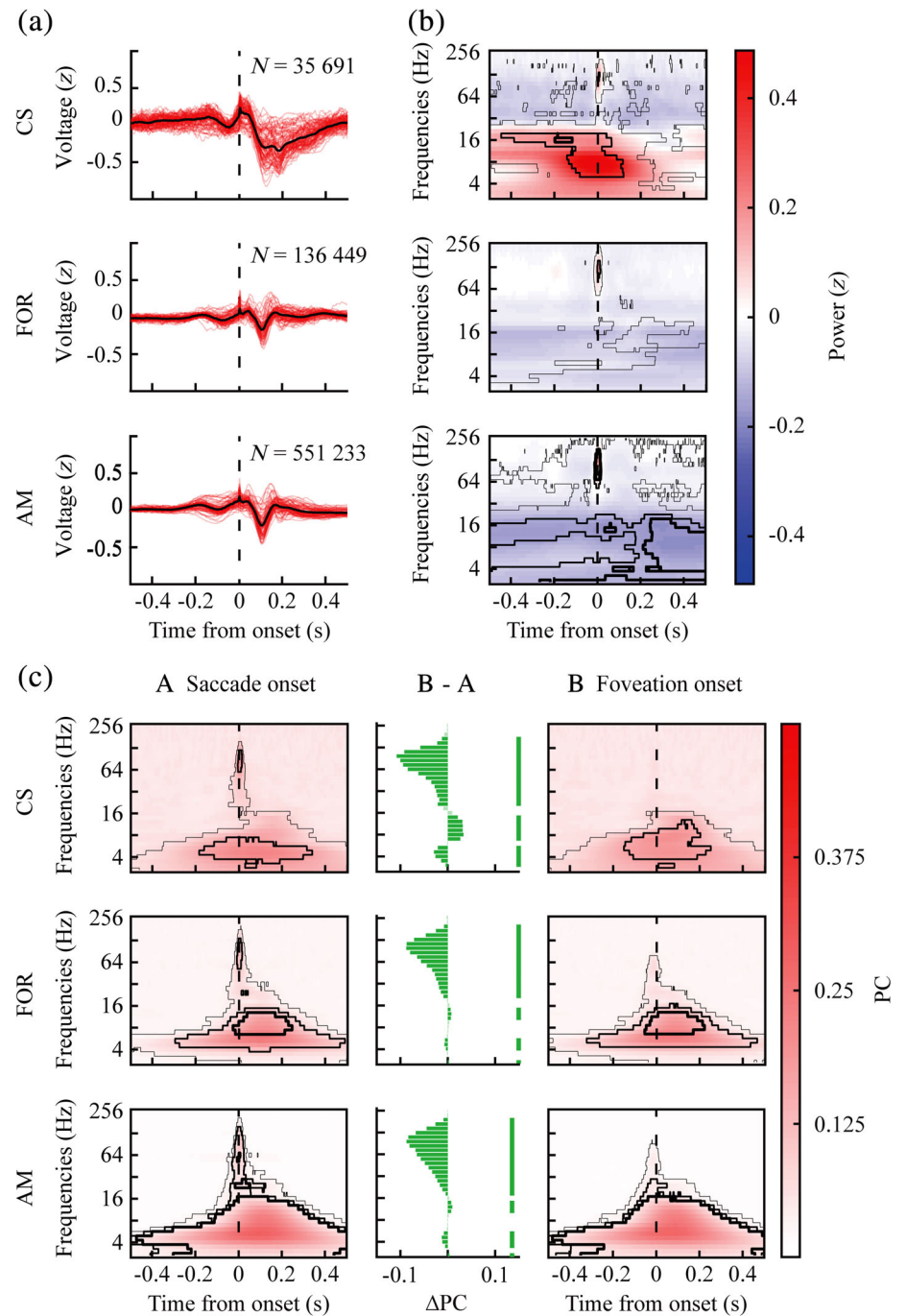


FIGURE 2 Trial averaged behavioral and local field potential (LFP) data. Averaged saccade probability (top), z-scored local field potential (LFP; black line; middle), z-scored LFP power (middle) and intertrial phase clustering (PC) (bottom), around target onsets, for the Cued Saccade (CS; a), Foraging (FOR; b), and Associative Memory (AM; c) tasks. N indicates the total number of trials averaged across all electrodes (CS: 86; FOR: 82; AM: 91 electrodes). (d) Average power (left) and intertrial PC (bottom) differences between the first 500 ms posttarget and the last 500 ms pretarget, for each of the 34 wavelet center frequencies. Shaded areas indicate SD. Solid lines above the plot indicate statistical significance (paired t test, Bonferroni corrected, $p < .05/34$ frequencies)

FIGURE 3 Saccade and foveation onset-triggered LFPs. (a) Averaged saccade onset-triggered z-scored local field potential (LFP) traces within each electrode (red traces) and cross-electrode grand average (black traces). (b) Saccade onset-triggered z-scored LFP power. (c) Saccade onset (left) and foveation onset (right) triggered phase clustering and their peak differences (ΔPC , center). Black outlines illustrate the proportion of significant electrodes, where thin: >5%, middle: >50%, and thick: >75%, computed from nonparametric permutation testing within electrode ($p < .01$, pixel-based correction for multiple comparisons). Dark green bars and vertical line indicate statistical significance of a paired t test ($p < .05$, Bonferroni corrected)



influenced by saccade probability, whereas low-frequency LFP power seemed modulated by task.

3.1 | Saccade evoked changes in LFP power and PC

We computed saccade-triggered LFPs (Figure 3a) and power (Figure 3b), as well as saccade and foveation-triggered PC (Figure 3c), including all on-screen saccades within each task. As anticipated, event-related responses were visible in the LFP traces (Figure 3a, red trace: single-electrode average; black trace: grand average across electrodes) and mostly contained within the first 200 ms after saccade onset (Hoffman et al., 2013; Jutras et al., 2013; Sobotka & Ringo, 1997).

Investigation of saccade-triggered LFP power confirmed a gamma band power increase at the time of saccade onset. This increase was significant for 52, 74, and 96% of all electrodes during the CS, FOR, and AM tasks, respectively (Figure 3b, black outlines: thin >5%; middle >50%; thick: > 75% of all electrodes showed significance). Conversely, low-frequency power displayed a heterogeneous pattern across tasks. Despite having over 45% of all channels showing significant power modulation around saccade times for frequencies below 20 Hz, the sign of the modulation was not consistent across tasks (Figure 3b). The median z-transformed power within the first 200 ms was greater than 0 for each frequency band below 20 Hz during the CS task, and lower than 0 for the FOR and AM tasks (sign test, $p < .001$ for all conditions).

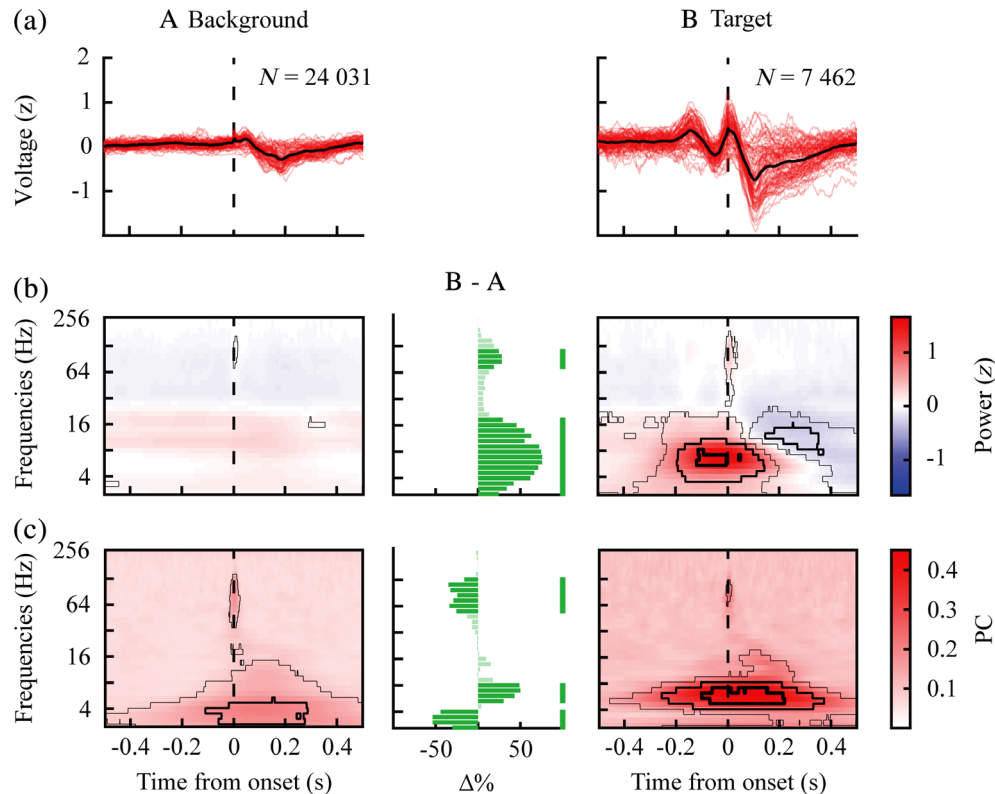


FIGURE 4 Comparison of saccades to visual targets and grey background-triggered LFPs. (a) Averaged z-scored local field potential (LFP) traces within each electrode (red traces) and cross-electrode grand average (black trace); (b) z-scored LFP power; and (c) phase clustering (PC) for all saccades landing on a uniform grey screen (background) or on a fixation target (target) during the Cued Saccade task. *N* values indicate the total number of saccades. Black outlines illustrate the proportion of significant electrodes, where thin: >5%, middle: >50%, and thick: >75%, computed from nonparametric permutation testing within electrode ($p < .01$, pixel-based correction for multiple comparisons). Proportions of significant electrodes were compared (B-A) for power (B) and PC (C) values via a chi-square test for equality of proportions and are labelled as proportion differences ($\Delta\%$). Dark green bars highlight significant differences, $p < .05$ Bonferroni corrected

Next, we explored PC values following saccade and foveation onsets (saccade landing; Figure 3c, first and last columns) and computed their difference across frequency bands. Gamma band PC was significantly greater for saccade onsets, regardless of task (Figure 3c, column B-A). Low-frequency patterns were highly similar across tasks: frequencies in the alpha/beta range of 8–16 Hz were significantly more clustered around fixation onsets, whereas frequencies around ~4–6 Hz were significantly more clustered around saccade onsets (Figure 3c, middle column).

Taken together, these results indicate that the patterns of saccade/fixation onset-triggered PC, as well as their relative differences, were consistent across tasks. They also suggest a frequency-specific modulation of hippocampal LFPs by the sensory and motor components of saccade-fixation sequences.

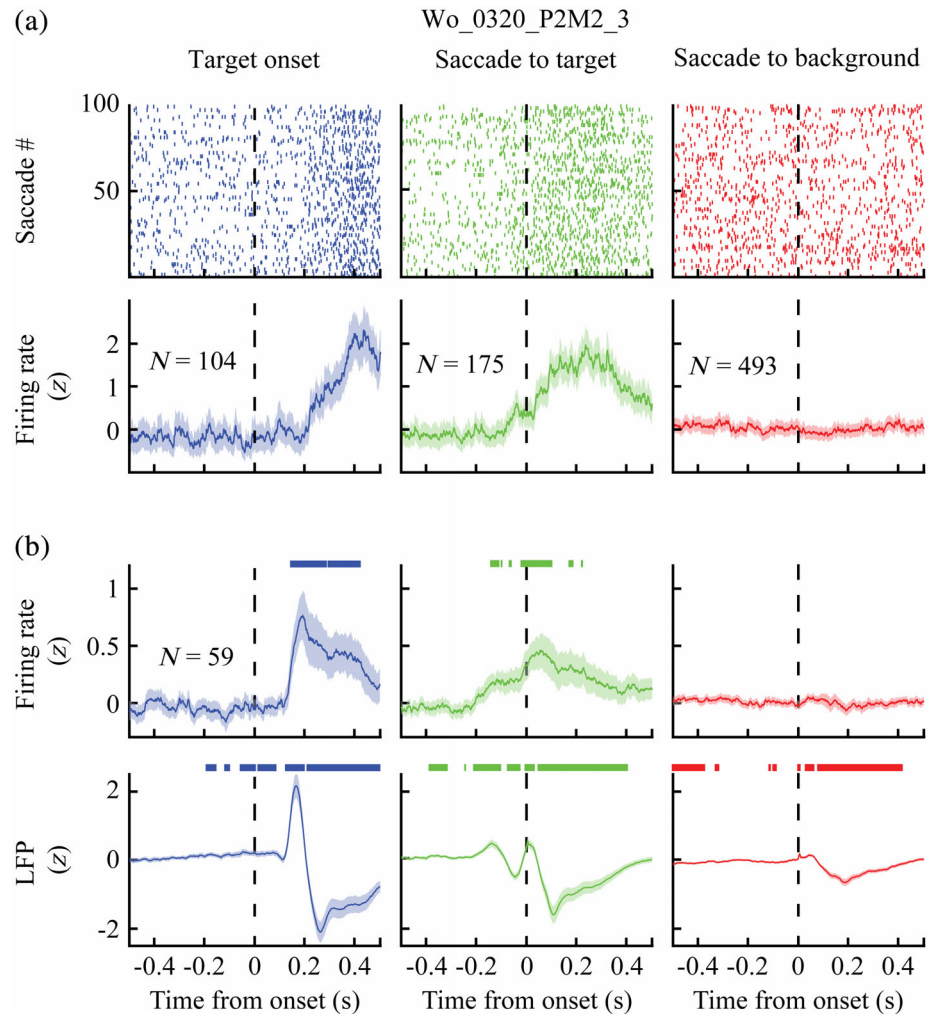
3.2 | Contributions of stimulus onsets and saccade signals to LFP power and PC

During visually guided saccades, the contributions of the visual stimulus and saccade command to the neural response are difficult to dissociate because saccades occur right after the visual stimulus onset.

However, during the CS task, the animals made two types of saccades: spontaneous saccades across the uniform grey background when no stimuli were on screen, and saccades from the uniform background to appearing visual targets. Thus, by analyzing the electrical activity in both conditions it would be possible to isolate the contribution of saccades and the added contribution visual stimulus onsets.

We first computed the distributions of saccade amplitudes, directions, durations, and intersaccade intervals (ISIs) for saccades to the background ($N = 24,031$) and to the fixation point ($N = 7,462$; Figure S1a). Despite targets being positioned near the edges of the screen (see Section 2), a large proportion of target saccades were of small amplitude (median amplitude background: 9.33 DVA; target: 3.08 DVA). This could be explained by the animals rapidly making large amplitude saccades to the appearing targets, followed by small corrective saccades inside the fixation window. Saccades to the blank background were mostly rightward, of longer duration (median duration background: 38 ms; target 24 ms, $p < .001$ rank-sum test) and less frequent (median ISI background: 626 ms, target: 204 ms; $p < .001$ rank-sum test) than visually guided saccades to the fixation target.

FIGURE 5 Firing rate changes evoked by visual targets and saccades. (a) Single unit example of spiking modulations around stimulus onset (left column) and saccade onsets to the appearing target (center column) and uniform background (right column). Top row presents the first 100 single event raster for all conditions. Bottom row shows the averaged spike density function for each condition. (b) Averaged spike density function (top row) over all electrodes, where all threshold crossings were pooled as a single multiunit cluster within each electrode. Bottom row presents the averaged LFP traces from the same electrodes. All data were z-score normalized to a baseline period of -500 to -200 ms preevent onset. Solid lines above the plots indicate significant difference from 0 (t test, $p < .05/1,000$ samples)



Gamma power at saccade onset was increased across 21% of electrodes for saccades to the background, and 45% of electrodes for saccades to the target (Figure 4b). Low-frequency power fluctuations were significant in less than 5% of electrodes for saccades to the background (Figure 4b-A), and 78% of electrodes for saccades to targets (Figure 4b-B). Consistently, LFP power was modulated on a larger proportion of electrodes during saccades to the target than during saccades to the background (Figure 4b, column B-A); chi-square test for equality of proportions, see Section 2).

Different from power modulations, gamma band PC was significantly greater than chance for both saccades to a target (15% of electrodes; Figure 4c) and saccades to the background (45% of electrodes). In the low frequencies, background saccades showed significant PC values around 4 Hz (70% of electrodes) while saccades to targets showed their significant PC values almost exclusively between 4 and 8 Hz (81% of electrodes), with less than 20% of electrodes showing significance for frequencies below 4 Hz.

These results indicate that saccades across a uniform background are sufficient to elicit PC in the hippocampus. Saccadic modulation of LFPs appeared quantitatively different between saccades to the uniform background and to fixation targets. Factors that may contribute to these differences are the visual inputs produced by the appearance

of the target and/or the future reward associated with saccades landing on the target.

3.3 | Effects of visual transients and saccades on local spiking activity

One of our original hypotheses predicted that signals linked to saccades (e.g., efference copy of the saccade command) would produce PC in the hippocampus and modulate the sensitivity of neurons to visual inputs. If this is the case, neurons should become less responsive during saccades and more responsive to visual inputs following saccades. We quantified single-unit activity around target onsets (Figure 5a, first column), saccades to the target (second column), and saccades to the background (third column). From the neuron in Figure 5a, we found that a clear increase in neuronal responses synchronized to target onsets, and to the onset of saccades to the target. The increase in firing rate visible in the spike density functions of the second row appears larger when responses are aligned to target onsets than when aligned to saccade onsets. This is likely due to some variability in the interval between target and saccade onsets (i.e., saccade response latency). Interestingly, no modulations were

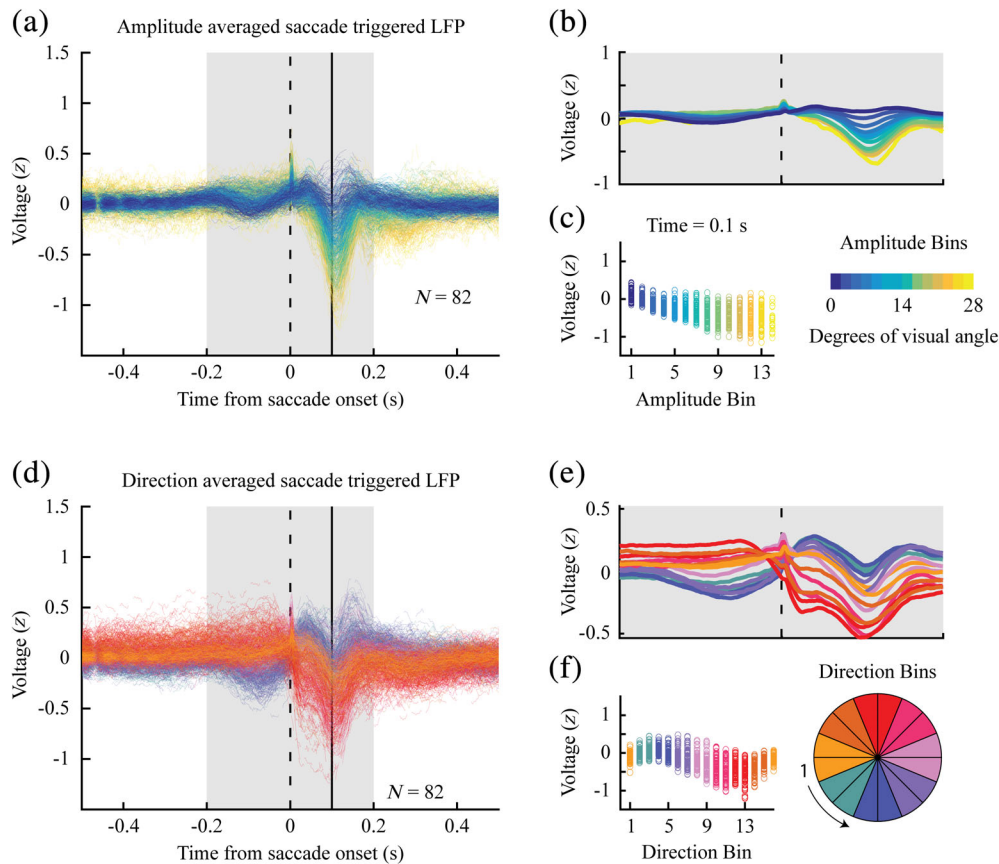


FIGURE 6 Saccade parameters correlation with LFP power. (a, d) Within electrode ($N = 82$) averaged local field potential (LFP) traces for each amplitude ($N = 14$; a) and direction ($N = 16$; d) bin around saccade onset (vertical dashed line). (b, e) Grand average across all electrodes within a 400-ms window (a, d, grey rectangle) centered on saccade onset. (c, f) Individual electrode values at 100 ms post saccade onset for each bin (a, d, solid black line)

found when we examined saccades to the background, suggesting that saccades alone did not influence the neuron's firing rate.

We combined all units within each electrode to obtain the average multiunit spiking responses. We also averaged LFP traces from the same electrodes (Figure 5b). As anticipated, robust effects on spikes and LFPs were found following target and saccade to target onsets (Figure 5b, first and second columns; t test against 0, $p < .05$, Bonferroni corrected). In contrast, saccades to the grey background triggered only LFP effects (Figure 5b, right column; t test against 0, $p < .05$, Bonferroni corrected), and no change in spiking activity (t test against 0, $p > .05$, Bonferroni corrected).

These results refute our initial hypothesis; signals related to saccades, likely of extra-hippocampal origin, cluster the phase of LFPs in the hippocampus without necessarily altering the spiking rate of single neurons. On the other hand, sensory signals, such as the ones evoked by target onsets, trigger spiking activity in hippocampal neurons. Our experiments cannot disentangle the effect of stimulus onsets from the one of saccades (i.e., test whether stimulus onsets alone or stimulus onsets and saccades evoke spiking activity). Nevertheless, they suggest a synergistic interaction between signals related to these two processes.

3.4 | Correlation between LFPs and saccade parameters

If saccade-related signals reach the hippocampus to influence LFPs, regardless of visual stimulation, one may find that the parameters of

the saccade (e.g., amplitude and direction) modulate the power and/or phase of LFP oscillations. To explore this issue, we pooled saccades from all tasks to obtain a large sample size, binned saccade amplitudes in 14 nonoverlapping bins (0–28 DVA, steps of 2 DVA), and computed the averaged saccade-triggered LFP trace for each bin (Figure 6a; single-electrode examples are presented in Figure S2). Interestingly, both the high-frequency peak at saccade onset (Figure 6a, b, vertical dashed line) and the negative deflection around 100 ms postsaccade (Figure 6a, c, solid black line) scaled with saccade amplitude ($p < 10^{-20}$, one-way analysis of variance [ANOVA] against amplitude bins).

As variations in the scale of averaged LFP deflections could be due to either changes in power or in the reliability of PC, we further characterized the relationship between saccade amplitude and LFP signal parameters via MLR (see Section 2). Regression coefficients were computed for the 400 ms around saccade initiation (± 200 ms), in nonoverlapping steps of 25 ms. The proportion of electrodes showing significant regression coefficients for LFP power and phase are illustrated in Figure S3a. The power of the mid-gamma peak at saccade onset significantly correlated with saccade amplitude on 98% of all electrodes, while power in the 6–8 Hz range at 100 ms postsaccade correlated with amplitude on 84% of all electrodes ($>50\%$ 4–8 Hz; $p < .001$, binomial test).

LFP phase was found to be significantly correlated with saccade amplitude in the gamma range (52%) and for virtually every frequency below 16 Hz ($>80\%$) over the entire 200 ms postonset epoch ($p < .001$, binomial test). However, when controlling for the possible effect of signal power on estimates of phase, we found this effect not

to be significant (see Figure S3b–e). Thus, the power, but not the phase, of the LFPs was correlated with saccade amplitude.

As a second control, to investigate the possibility of myogenic contamination in our recorded LFPs (Kovach et al., 2011), we compared the polarity of LFP deflections across the mediolateral axis (Hoffman et al., 2013), as polarity inversion across cell layers might not be as apparent in primates (Leonard et al., 2015). To do so, we compared simultaneously recorded electrodes spanning the mediolateral axis, with the same position along the anterior–posterior axis (Figure S4). For the three tested electrode pairs, saccades during the AM task generated deflections of opposite polarities in the averaged LFP trace (Figure S4, top) and in the 4–8 Hz filtered data (Figure S4, middle). We additionally compared the phase distributions (Figure S4, bottom) for individual saccades at 100 ms postonset (Figure S4, middle, solid black line), and found significant differences across mediolateral position ($p < .001$, Kuiper test; Berens, 2009). Thus, the isolated effects were unlikely to be caused by myogenic contamination.

We further examined whether saccade direction had a systematic relationship with the power or phase of hippocampal LFPs. We binned saccades into 16 consecutive bins of 22.5° . Bin-averaged LFP traces from individual electrodes are displayed in Figure 6D (single-electrode traces in Figure S2), while grand averages across electrodes are presented in Figure 6e. A striking difference in z-scored voltage values over all bins was visible at 100 ms postsaccade onset (Figure 6d,f, solid black line; $p < 10^{-20}$, one-way ANOVA against direction bins), peaking between downward saccades (blue) and upward saccades (red). Quantification of saccade direction and LFP phase correlation via MLR validated these findings, where 89% ($p < .001$, binomial test) of all electrodes presented a significant regression coefficient for oscillations lower than or equal to 4 Hz (Figure S5a). Furthermore, less than 10% ($p > .05$, binomial test) of electrodes showed significant regression parameters between power and saccade direction, regardless of time and frequency.

Considering the uneven distribution of saccade amplitudes across direction bins (Figure S3c), and the regression results between saccade amplitude and low-frequency LFP phase (Figure S3e), we replicated the MLR analysis on saccade directions within single amplitude bins. To avoid the confounding effect of saccade amplitude on phase, we selected only a single amplitude bin within the range of highest PC significance per electrode (bin numbers 4–9; Figure S3b, right). Single amplitude bins were selected to maximize the number of saccades within each direction bin. The distribution of selected amplitude bins is presented in Figure S5c. Regression results (Figure S5b) confirmed the confounding effect of saccade amplitude on MLR phase regression, showing virtually no relationship between saccade direction and gamma phase (<3% of electrodes over all time–frequency points, $p > .05$, binomial test), and a strong decrease in significance probability for frequencies above 5 Hz (<20%, $p < .001$, binomial test). On the other hand, 55% of all electrodes remained significant for frequencies lower or equal to 4 Hz ($p < .001$, binomial test). These results suggest that saccade direction is reliably correlated with the phase, and not power, of very low-frequency LFPs (≤ 4 Hz).

4 | DISCUSSION

4.1 | Changes in power and phase of LFP oscillations in primate hippocampus during saccades

Changes in the power of hippocampal oscillations have been associated with a broad range of cognitive operations such as learning, movement, and decision-making (Belchior, Lopes-dos-Santos, Tort, & Ribeiro, 2014; Hasselmo, 2005; Watrous, Fried, & Ekstrom, 2011), while changes in phase are seen as temporal coordinators of neuronal activity associated with memory formation (Colgin, 2016; Lisman & Jensen, 2013). Our results show distinct frequency-specific power profiles when LFPs were aligned to target onset across tasks. On the other hand, we found that PC seems to occur in similar frequencies regardless of task. Because saccades occur following target onset and are therefore a common denominator across tasks, our results may suggest that the power effects are caused by the idiosyncrasies of the different tasks, while the PC effects are likely linked to saccades. This may indicate a separation between cognitive and motor effects on hippocampal field potentials. These results agree with previous reports of dissociations between the power and phase of LFPs in the hippocampus (Givens, 1996; Hoffman et al., 2013; Jutras et al., 2013; Jutras & Buffalo, 2014; Rajkai et al., 2008; Schroeder & Lakatos, 2009).

Previous studies have proposed that hippocampal activity is modulated by task and contextually relevant information (Ekstrom & Ranganath, 2017; Loonis, Brincat, Antzoulatos, & Miller, 2017; McKenzie et al., 2016; Wirth et al., 2017). Some studies have also reported sensing or stimulus-related PC to be absent during tasks that are less likely to engage the hippocampus (Berg, Whitmer, & Kleinfeld, 2006; Givens, 1996; Hoffman et al., 2013; Jutras et al., 2013). In our study, we found significant PC following saccades, regardless of stimulus conditions and tasks. This effect occurred within frequency bands previously associated with explicit learning and relevant stimuli processing (i.e., delta/theta and alpha/beta; Brincat & Miller, 2015; Loonis et al., 2017) and despite minimal changes in visual stimulation.

4.2 | Frequency-specific PC by visual transient and saccades

We found that fixation and saccadic effects occurred in different frequency ranges. Recent work has cautioned against the a priori labeling and filtering of LFP data, while highlighting the lack of coherence in frequency selections (Einevoll, Kayser, Logothetis, & Panzeri, 2013; Herreras, 2016). Indeed, a broad range of frequencies have been arbitrarily identified as “classical” theta, anywhere between 3 and 12 Hz (Colgin, 2016; Ekstrom & Watrous, 2014; Jacobs, 2014; Killian, Jutras, & Buffalo, 2012; Skaggs et al., 2007). Moreover, comparable studies of saccade-triggered PC in the primate hippocampus have found significant results for minimally overlapping frequency ranges: 3–8 Hz (Hoffman et al., 2013) and 6–12 Hz (Jutras et al., 2013). The narrowly spaced complex Morlet wavelets used in this study have allowed us to identify three separable behavioral correlates within the “classical” theta range of 3–12 Hz. We will thus attempt to reconcile

these three phenomena within the previously described hippocampal literature and highlight the putatively different cognitive processes involved within each frequency band.

Firstly, we found that frequencies between 8 and 16 Hz, labelled as alpha/beta, were more strongly correlated with incoming sensory signals (foveation onset) than with saccades, regardless of condition. Consistently, multiple studies found significant correlations between the hippocampus and PFC LFPs following stimulus exploration, within the same frequencies. For example, Place, Farovik, Brockmann, and Eichenbaum (2016) simultaneously recorded from rodents' hippocampus and PFC and showed significant bidirectional phase coherence between 7 and 12 Hz within one second of contextual and target sampling. Interestingly, during contextual exploration hippocampal phase preceded PFC phase, while this relationship was reversed during target sampling. Similarly, Brincat and Miller (2015), as well as Loonis et al. (2017), measured a strong hippocampus led phase coherence between 9 and 16 Hz following correct trial outcome feedback in macaque monkeys. Although some results must be interpreted cautiously due to the lack of homology between rodent and primate PFC (Carlén, 2017; Kaas, 2013), they reveal a degree of generalization across mammalian brains.

Human intracranial recordings, albeit limited to the neocortex, also found significant PC between 6 and 13 Hz following stimulus onset, with the preferred phase varying between the encoding and retrieval epochs of the task (Rizzuto, Madsen, Bromfield, Schulze-Bonhage, & Kahana, 2006). Moreover, despite being classically defined in lower frequencies in rodents (i.e., 4–9 Hz), a strong parallel can be drawn between our findings and the “sensory processing” Type 2 theta oscillation (Bland & Oddie, 2001; Gangadharan et al., 2016; Kramis, Vanderwolf, & Bland, 1975; Sainsbury, Harris, & Rowland, 1987). Future studies investigating the directionality and information content of saccade-triggered alpha/beta interactions between hippocampus and PFC in primates are still required to validate this hypothesis.

Secondly, we found that frequencies in the central region of the classical theta, between 4 and 8 Hz, presented strong PC aligned to the onset of saccades, whose power reliably correlated with saccade amplitudes. Considering that gaze location within an environment can elicit responses in the primate hippocampus (Rolls et al., 1997; Rolls & O'Mara, 1995; Wirth et al., 2017), strong parallels between gaze exploration and rodent locomotion have been drawn (Killian et al., 2012; Rolls & Wirth, 2018; Sobotka & Ringo, 1997). Accordingly, classical theta band power has been repeatedly correlated with locomotion speed (Bland & Oddie, 2001; Ekstrom & Watrous, 2014) and encodes distance travelled by abrupt displacements, namely jumping or teleportation, in both rodents and humans (McNaughton, Battaglia, Jensen, Moser, & Moser, 2006; Vass et al., 2016). Interestingly, Vass et al. (2016) demonstrated that this effect occurs without visual input during teleportation, suggesting an internal representation of space independent from visual, vestibular, and self-motion cues. Our data are in accordance with these models, where the magnitude of abrupt displacements in gaze position (i.e., saccades) correlated with theta power.

Lastly, we showed that the delta band (≤ 4 Hz) phase correlated with saccade direction, independent of power (Figures 6 and S5). These results validate the findings of Sobotka, Nowicka, and Ringo (1997) which found infrequent, yet highly significant, differences in evoked responses of right versus left saccades. Saccade direction modulation of delta phase seemed to be dominated by differences in upward versus downward saccades, where upward saccades were related to the falling edge of the low-frequency oscillation, whereas downward saccades were related to rising edge (Figure 6e,f). Considering the visual perspective of the real and virtual worlds, as well as the quasilinear shape of the maze, upward saccades typically shift gaze farther in the environment, while downward saccades bring gaze closer to the subject. Analogously, place cell firing in animals has been repeatedly correlated with the phase of classical theta oscillations with regard to where within a place field the animal is, a process termed phase precession. During this process, place cells' spiking correlates with late, or rising edge, phase when animals enter the place field, and correlates with early, or falling edge, phase when animals leave the place field (Dragoi & Buzsáki, 2006; O'Keefe & Recce, 1993). Studies on the functional role of phase precession have further hypothesized its involvement in attention to either proximal or distal cues (Fenton et al., 2010) or in prospective versus retrospective position encoding (Bieri, Bobbitt, & Colgin, 2014; Lisman & Redish, 2009). In our data, near and distant spatial processing correlates, respectively, with late and early theta phase suggesting a relationship between these variables.

4.3 | Origin of LFP modulations

One may ask whether hippocampal LFPs are directly modulated by saccade signals (e.g., efference copy signals reaching the hippocampus) or whether it is an indirect effect of upstream visual areas modulation (e.g., saccadic suppression). Unlike spikes, LFPs are notoriously difficult to interpret due to the uncertainty in their source localization (i.e., the inverse problem) and spatial spread (Buzsáki, Anastassiou, & Koch, 2012; Herreras, 2016; Katzner et al., 2009).

We found that single neuron responses increased after visual transients and saccades to visual transients, but not after saccades within a uniform visual field. These effects contrast with those reported by previous studies in other areas. For example, within V1, saccades trigger a biphasic suppression-enhancement effect on neuronal activity (Burr et al., 1994; McFarland et al., 2015). This modulation is consistent across most recorded units, remains during saccades in darkness and with minimal changes in retinal stimulation (McFarland et al., 2015). This latter trend was absent in our data. Similarly, only a subset of hippocampal neurons are modulated by saccades (Andrillon et al., 2015) and their responses, including saccade direction encoding (Gulli et al., 2018), greatly differ from the typical V1 biphasic one (Andrillon et al., 2015; Killian et al., 2015; Ringo et al., 1994; Sobotka et al., 1997).

Saccades have been shown to modulate LFPs in multiple brain areas, such as PFC (Tremblay et al., 2015) and visual cortex (Ito et al., 2011, 2013; Staudigl et al., 2017) cortices. In V1, both saccades and fixations have been found to elicit PC in the delta/theta and

alpha/beta bands (Ito et al., 2011, 2013). Interestingly, phase preferences for both events are inverted across regions, where hippocampal phase is preferentially clustered by saccade onsets in the theta band and by foveation onsets in the alpha/beta band, whereas the opposite is true for V1 (Ito et al., 2011, 2013). The numerous differences identified imply a different role of eye movements within each area. For example, saccadic modulation within visual areas is hypothesized to reduce interference between presaccadic and postsaccadic stimuli (Burr et al., 1994; McFarland et al., 2015). Conversely, within the hippocampus, modulation of single neurons and LFPs by saccade directions and amplitudes (Figure 6) may serve to link the presaccadic and postsaccadic stimuli into a unified memory representation.

In general, our results suggest that visual transients evoke both PC and increases in the responses of hippocampal neurons. On the other hand, saccades in the dark evoke PC but do not produce spiking activity in hippocampal neurons. This is compatible with both hypotheses, where motor signals, reflected in stimuli-independent correlations of saccade parameters with the delta and theta bands, reach the hippocampus to process sensorimotor and/or spatial computations, and to possibly prepare the hippocampus for subsequent sensory signals. Consequently, sensory and/or cognitive signals, reflected in alpha/beta band PC and increased spiking activity, reach the hippocampus following foveation onsets to possibly associate sensory information with spatiotemporal computations.

4.4 | Myogenic contamination

Recent studies have challenged the “local” extent of LFPs (Canolty et al., 2010; Herreras, 2016; Kajikawa & Schroeder, 2011), raising the question of whether the measured correlations with saccade parameters could reflect eye muscle artifacts or signals coming from neighboring structures, such as the thalamus. While the gamma band effect we measured here is likely due to myogenic contamination (Katz et al., 2018; Kovach et al., 2011), we have several reasons to believe that this is not the case for the low-frequency effects. Firstly, similar to (Hoffman et al., 2013), our effects occurred well after the offset of eye movements, in low frequencies not associated with myogenic contamination and were modulated by task. Secondly, the magnitude of myogenic artifacts is modulated across ipsiversive and contraversive saccades, whereas our data do not show a correlation between LFP magnitude and saccade direction. Thirdly, in primates hippocampal LFP polarity reverses along the mediolateral axis (Hoffman et al., 2013), and possibly not across cellular laminae (Leonard et al., 2015) as is the case in rodents, a trend found across simultaneously recorded electrode pairs spanning the mediolateral axis (Figure S4). Lastly, regarding possible thalamic contamination, where neurons encode efference copy signals for saccades (Sommer & Wurtz, 2006), as far as we know these cells do not encode saccade amplitudes in their firing rate. In other words, similar firing rates across different amplitudes would yield similar activity states and most likely similar power values. It is therefore improbable that myogenic contamination was limited to the theta band, while not affecting the delta and alpha/beta neighboring bands.

4.5 | Relationship to previous studies

We found significant saccade-related PC in the hippocampus during all tasks, while Hoffman et al. (2013) only found PC during active vision, but not during the intertrial interval, and Jutras et al. (2013) found no significant PC for visually guided saccades to a fixation cross. This could be explained by differences in task design, as well as in the methods we used to detect both saccades and phase modulations. Although we found significant PC across all tasks, it was weakest during saccades to the blank screen in the CS task. This may be due to self-generated saccades in the dark being typically of smaller amplitude (Andrews & Coppola, 1999) and of slower speed (Helmchen, Straube, & Büttner, 1994; Sobotka & Ringo, 1997) when compared to saccades made during complex scenes viewing. Indeed, in our data, over 30% of all saccades to the background during the CS task were shorter than 3 DVA (Figure S1).

The lack of significant PC following visually guided saccades in Jutras et al. (2013) could be explained by the fact that the authors discarded the last 100 ms before the saccade and the first 400 ms after it; we focused our analyses on the first 500 ms following saccade onsets, when a signal corresponding to the saccade command could reach cortical and subcortical areas. Although the authors in Jutras et al., (2013) specifically discarded this epoch to effectively avoid visual transient contamination, ours and other studies have identified a narrow temporal window for PC following saccades between 100 and 300 ms (Hoffman et al., 2013; Sobotka & Ringo, 1997).

While we cannot rule out the possibility that the significant PC measured for target saccades during the CS task is entirely due to the target onset, the presence of reliable PC for saccades to the uniform background argues otherwise. Lastly, we found that the motor component of saccades was reflected in a narrow band ~4–8 Hz, whereas the authors in (Jutras et al., 2013) band-pass filtered the LFPs between 6 and 12 Hz, possibly adding noninformative frequencies and reducing signal strength.

4.6 | Physiological role of saccade-triggered LFP modulations

Our results suggest that signals linked to saccade commands and visual stimuli reach the hippocampus, producing frequency-specific synchronization of LFPs. Considering the role of the hippocampus in associative memory formation, where spatial, stimulus and contextual associations are sparsely encoded by neurons, it is possible that the frequency-specific saccade-triggered LFP modulations highlighted in this work could represent the various input and local computations required for this function. For example, delta band PC, more prominent during saccades to a uniform background (Figure 4), could reflect prospective processes as animals search the local visual space, awaiting the appearance of the next fixation target. Following target onset, its location information could be processed and reach the hippocampus via saccade amplitude correlated theta band power, yielding stronger power and PC within that band (Figure 4). For tasks requiring extensive stimuli sampling, such as our virtual reality tasks,

the influence of local and remote stimulus-related processing could occur within the alpha/beta band. There are however two important points to consider in order to reconcile this hypothesis with the absence of neuronal modulation for the background condition of the CS task (Figure 5).

First, the multiple signals represented by these LFP bands might not be sufficient to elicit hippocampal spiking activity in the absence of stimuli. For saccades within a uniform field of view, prospective reward or relative spatial position are meaningless. Moreover, visually evoked neuronal firing could simply be coordinated by LFPs; in this case, a physiological role for LFPs would be undetectable without stimuli to induce neuronal firing. For example, during phase precession, neurons are not activated if the animal is outside its place field, even in the presence of strong theta activity. Saccade-triggered LFPs could thus serve a similar role. Secondly, while it is possible that some neurons were activated following saccades, their sparse firing and complex nonlinear tuning might hinder their detection when pooled with every other neuron recorded on the same electrode, as is the case in our analyses.

These findings support the hypothesis that, in primates, saccade commands serve as facilitators of sensory inputs activating hippocampus neuronal networks to enact memory formation. Further work is required to investigate the influence of specific LFP frequency bands on the neuronal representations of visual targets, their values, positions, and subsequent associative memory formation, around consecutive saccade-fixation cycles.

ACKNOWLEDGMENTS

We thank Matthew Leavitt and Sebastien Tremblay for critical input and discussion, and all members of the J.C.M.T. lab for support. We thank Blandine Bally, Kevin Barker, Sara Chisling, Steve Frey, Steve Nuara, and Walter Kucharski for technical assistance.

DATA ACCESSIBILITY

Data available on request from the authors.

ORCID

Guillaume Doucet  <https://orcid.org/0000-0003-2260-1002>

Roberto A. Gulli  <https://orcid.org/0000-0001-5983-0672>

REFERENCES

- Andrews, T. J., & Coppola, D. M. (1999). Idiosyncratic characteristics of saccadic eye movements when viewing different visual environments. *Vision Research*, 39(17), 2947–2953. [http://doi.org/10.1016/S0042-6989\(99\)00019-X](http://doi.org/10.1016/S0042-6989(99)00019-X)
- Andrillon, T., Nir, Y., Cirelli, C., Tononi, G., & Fried, I. (2015). Single-neuron activity and eye movements during human REM sleep and awake vision. *Nature Communications*, 6, 1–10. <http://doi.org/10.1038/ncomms8884>
- Bartlett, A. M., Ovaysikia, S., Logothetis, N. K., & Hoffman, K. L. (2011). Saccades during object viewing modulate oscillatory phase in the superior temporal sulcus. *Journal of Neuroscience*, 31(50), 18423–18432. <http://doi.org/10.1523/JNEUROSCI.4102-11.2011>
- Belchior, H., Lopes-dos-Santos, V., Tort, A. B. L., & Ribeiro, S. (2014). Increase in hippocampal theta oscillations during spatial decision making. *Hippocampus*, 24(6), 693–702. <http://doi.org/10.1002/hipo.22260>
- Berens, P. (2009). CircStat: A MATLAB toolbox for circular statistics. *Journal of Statistical Software*, 31(10), 1–21. <http://doi.org/10.1002/wics.10>
- Berg, R. W., Whitmer, D., & Kleinfeld, D. (2006). Exploratory whisking by rat is not phase locked to the hippocampal theta rhythm. *Journal of Neuroscience*, 26(24), 6518–6522. <http://doi.org/10.1523/JNEUROSCI.0190-06.2006>
- Bieri, K. W., Bobbitt, K. N., & Colgin, L. L. (2014). Slow and fast gamma rhythms coordinate different spatial coding modes in hippocampal Place cells. *Neuron*, 82(3), 670–681. <http://doi.org/10.1016/j.neuron.2014.03.013>
- Bland, B. H., & Oddie, S. D. (2001). Theta band oscillation and synchrony in the hippocampal formation and associated structures: The case for its role in sensorimotor integration. *Behavioural Brain Research*, 127(1–2), 119–136. [http://doi.org/10.1016/S0166-4328\(01\)00358-8](http://doi.org/10.1016/S0166-4328(01)00358-8)
- Brainard, D. H. (1997). The psychophysics toolbox. *Spatial Vision*, 10(4), 433–436. <http://doi.org/10.1163/156856897X00357>
- Brincat, S. L., & Miller, E. K. (2015). Frequency-specific hippocampal-prefrontal interactions during associative learning. *Nature Neuroscience*, 18(4), 1–10. <http://doi.org/10.1038/nn.3954>
- Buffalo, E. A. (2015). Bridging the gap between spatial and mnemonic views of the hippocampal formation. *Hippocampus*, 6(March), 1–6. <http://doi.org/10.1002/hipo.22444>
- Burr, D. C., Morrone, M. C., & Ross, J. (1994). Selective suppression of the magnocellular visual pathway during saccadic eye movements. *Nature*, 371(6497), 511–513. <http://doi.org/10.1038/371511a0>
- Buschman, T. J., & Miller, E. K. (2007). Top-down versus bottom-up control of attention in the prefrontal and posterior parietal cortices. *Science*, 315(5820), 1860–1862. <http://doi.org/10.1126/science.1138071>
- Buzsáki, G., Anastassiou, C. a., & Koch, C. (2012). The origin of extracellular fields and currents—EEG, ECoG, LFP and spikes. *Nature Reviews Neuroscience*, 13(6), 407–420. <http://doi.org/10.1038/nrn3241>
- Canolty, R. T., Ganguly, K., Kennerley, S. W., Cadieu, C. F., Koepsell, K., Wallis, J. D., & Carmena, J. M. (2010). Oscillatory phase coupling coordinates anatomically dispersed functional cell assemblies. *Proceedings of the National Academy of Sciences*, 107(40), 17356–17361. <http://doi.org/10.1073/pnas.1008306107>
- Carlén, M. (2017). What constitutes the prefrontal cortex? *Science*, 358(6362), 478–482. <http://doi.org/10.1126/science.aan8868>
- Cohen, M. X. (2014). *Analyzing neural time series data*. MIT Press, Cambridge.
- Colgin, L. L. (2016). Rhythms of the hippocampal network. *Nature Reviews Neuroscience*, 17(4), 239–249. <http://doi.org/10.1038/nrn.2016.21>
- Corrigan, B. W., Gulli, R. A., Doucet, G., & Martinez-Trujillo, J. C. (2017). Characterizing eye movement behaviors and kinematics of non-human primates during virtual navigation tasks. *Journal of Vision*, 17(12), 1–22. <http://doi.org/10.1167/17.12.15>
- Doucet, G., Gulli, R. A., & Martinez-Trujillo, J. C. (2016). Cross-species 3D virtual reality toolbox for visual and cognitive experiments. *Journal of Neuroscience Methods*, 266, 84–93. <http://doi.org/10.1016/j.jneumeth.2016.03.009>
- Dragoi, G., & Buzsáki, G. (2006). Temporal encoding of place sequences by hippocampal cell assemblies. *Neuron*, 50(1), 145–157. <http://doi.org/10.1016/j.neuron.2006.02.023>

- Eichenbaum, H. (2004). Hippocampus: Cognitive processes and neural representations that underlie declarative memory. *Neuron*, 44(1), 109–120. <http://doi.org/10.1016/j.neuron.2004.08.028>
- Eichenbaum, H., & Cohen, N. J. (2014). Can we reconcile the declarative memory and spatial navigation views on hippocampal function? *Neuron*, 83(4), 764–770. <http://doi.org/10.1016/j.neuron.2014.07.032>
- Einevoll, G. T., Kayser, C., Logothetis, N. K., & Panzeri, S. (2013). Modelling and analysis of local field potentials for studying the function of cortical circuits. *Nature Reviews, Neuroscience*, 14(11), 770–785. <http://doi.org/10.1038/nrn3599>
- Ekstrom, A. D., & Ranganath, C. (2017). Space, time, and episodic memory: The hippocampus is all over the cognitive map. *Hippocampus*, 28, 1–16. <http://doi.org/10.1002/hipo.22750>
- Ekstrom, A. D., & Watrous, A. J. (2014). Multifaceted roles for low-frequency oscillations in bottom-up and top-down processing during navigation and memory. *NeuroImage*, 85(02), 667–677. <http://doi.org/10.1016/j.neuroimage.2013.06.049>
- Feigenbaum, J. D., & Rolls, E. T. (1991). Allocentric and egocentric spatial information processing in the hippocampal formation of the behaving primate. *Psychobiology*, 19(1), 21–40. <http://doi.org/10.1007/BF03337953>
- Fell, J., Dietl, T., Grunwald, T., Kurthen, M., Klaver, P., Trautner, P., ... Fernández, G. (2004). Neural bases of cognitive ERPs: More than phase reset. *Journal of Cognitive Neuroscience*, 16(9), 1595–1604. <http://doi.org/10.1162/0898929042568514>
- Fenton, A. A., Lytton, W. W., Barry, J. M., Lenck-Santini, P. P., Zinyuk, L. E., Kubik, S., ... Olypher, A. V. (2010). Attention-like modulation of hippocampus place cell discharge. *Journal of Neuroscience*, 30(13), 4613–4625. <http://doi.org/10.1523/JNEUROSCI.5576-09.2010>
- Frank, D. W., & Sabatinelli, D. (2017). Primate visual perception: Motivated attention in naturalistic scenes. *Frontiers in Psychology*, 8, 1–7. <http://doi.org/10.3389/fpsyg.2017.00226>
- Gangadharan, G., Shin, J., Kim, S.-W., Kim, A., Paydar, A., Kim, D.-S., ... Shin, H.-S. (2016). Medial septal GABAergic projection neurons promote object exploration behavior and type 2 theta rhythm. *Proceedings of the National Academy of Sciences*, 113(23), 6550–6555. <http://doi.org/10.1073/pnas.1605019113>
- Georges-François, P., Rolls, E. T., & Robertson, R. G. (1999). Spatial view cells in the primate hippocampus: Allocentric view not head direction or eye position or place. *Cerebral Cortex*, 9(3), 197–212. <http://doi.org/10.1093/cercor/9.3.197>
- Givens, B. (1996). Stimulus-evoked resetting of the dentate theta rhythm: Relation to working memory. *Neuroreport*, 8(1), 159–163. <http://doi.org/10.1097/00001756-199612200-00032>
- Gottlieb, J., Hayhoe, M., Hikosaka, O., & Rangel, A. (2014). Attention, reward, and information seeking. *Journal of Neuroscience*, 34(46), 15497–15504. <http://doi.org/10.1523/JNEUROSCI.3270-14.2014>
- Gulli, R. A., Duong, L., Corrigan, B. W., Doucet, G., Williams, S., Fusi, S., & Martinez-Trujillo, J. C. (2018). Flexible coding of memory and space in the primate hippocampus during virtual navigation. *BioRxiv*, 295774, 1–50. <http://doi.org/10.1101/295774>
- Hasselmo, M. E. (2005). What is the function of hippocampal theta rhythm? Linking behavioral data to phasic properties of field potential and unit recording data. *Hippocampus*, 15(7), 936–949. <http://doi.org/10.1002/hipo.20116>
- Helmchen, C., Straube, A., & Büttner, U. (1994). Saccade-related activity in the fastigial oculomotor region of the macaque monkey during spontaneous eye movements in light and darkness. *Experimental Brain Research*, 98(3), 474–482. <http://doi.org/10.1007/BF00233984>
- Herreras, O. (2016). Local field potentials: Myths and misunderstandings. *Frontiers in Neural Circuits*, 10, 1–16. <http://doi.org/10.3389/fncir.2016.00101>
- Hoffman, K. L., Dragan, M. C., Leonard, T. K., Micheli, C., Montefusco-Siegmund, R., & Valiante, T. A. (2013). Saccades during visual exploration align hippocampal 3–8 Hz rhythms in human and non-human primates. *Frontiers in Systems Neuroscience*, 7, 1–10. <http://doi.org/10.3389/fnsys.2013.00043>
- Hughes, A. M., Whitten, T. A., Caplan, J. B., & Dickson, C. T. (2012). BOSC: A better oscillation detection method, extracts both sustained and transient rhythms from rat hippocampal recordings. *Hippocampus*, 22(6), 1417–1428. <http://doi.org/10.1002/hipo.20979>
- Ibbotson, M. R., Crowder, N. A., Cloherty, S. L., Price, N. S. C., & Mustari, M. J. (2008). Saccadic modulation of neural responses: Possible roles in saccadic suppression, enhancement, and time compression. *Journal of Neuroscience*, 28(43), 10952–10960. <http://doi.org/10.1523/JNEUROSCI.3950-08.2008>
- Ito, J., Maldonado, P., & Grün, S. (2013). Cross-frequency interaction of the eye-movement related LFP signals in V1 of freely viewing monkeys. *Frontiers in Systems Neuroscience*, 7, 1–11. <http://doi.org/10.3389/fnsys.2013.00001>
- Ito, J., Maldonado, P., Singer, W., & Grün, S. (2011). Saccade-related modulations of neuronal excitability support synchrony of visually elicited spikes. *Cerebral Cortex*, 21(11), 2482–2497. <http://doi.org/10.1093/cercor/bhr020>
- Jacobs, J. (2014). Hippocampal theta oscillations are slower in humans than in rodents: Implications for models of spatial navigation and memory. *Philosophical Transactions of the Royal Society of London. Series B, Biological Sciences*, 369(1635), 1–9. <http://doi.org/10.1098/rstb.2013.0304>
- Jutras, M. J., & Buffalo, E. A. (2014). Oscillatory correlates of memory in non-human primates. *NeuroImage*, 85(Pt 2), 694–701. <http://doi.org/10.1016/j.neuroimage.2013.07.011>
- Jutras, M. J., Fries, P., & Buffalo, E. A. (2013). Oscillatory activity in the monkey hippocampus during visual exploration and memory formation. *Proceedings of the National Academy of Sciences*, 110(32), 13144–13149. <http://doi.org/10.1073/pnas.1302351110>
- Kaas, J. H. (2013). The evolution of brains from early mammals to humans. *Wiley Interdisciplinary Reviews: Cognitive Science*, 4(1), 33–45. <http://doi.org/10.1002/wcs.1206>
- Kajikawa, Y., & Schroeder, C. E. (2011). How local is the local field potential? *Neuron*, 72(5), 847–858. <http://doi.org/10.1016/j.neuron.2011.09.029>
- Katz, C., Patel, K., Talakoub, O., Hoffman, K., & Valiante, T. A. (2018). Differential generation of saccade, fixation and image onset event-related potentials in the human mesial temporal lobe. *BioRxiv*, 442855, 1–23. <https://doi.org/10.1101/442855>
- Katzner, S., Nauhaus, I., Benucci, A., Bonin, V., Ringach, D. L., & Carandini, M. (2009). Local origin of field potentials in visual cortex. *Neuron*, 61(1), 35–41. <http://doi.org/10.1016/j.neuron.2008.11.016>
- Kelly, R. C., Smith, M. A., Samonds, J. M., Kohn, A., Bonds, A. B., Movshon, J. A., & Lee, T. S. (2007). Comparison of recordings from microelectrode arrays and single electrodes in the visual cortex. *The Journal of Neuroscience : The Official Journal of the Society for Neuroscience*, 27(2), 261–264. <http://doi.org/10.1523/JNEUROSCI.4906-06.2007>
- Killian, N. J., Jutras, M. J., & Buffalo, E. A. (2012). A map of visual space in the primate entorhinal cortex. *Nature*, 491(7426), 761–764. <http://doi.org/10.1038/nature11587>
- Killian, N. J., Potter, S. M., & Buffalo, E. A. (2015). Saccade direction encoding in the primate entorhinal cortex during visual exploration. *Proceedings of the National Academy of Sciences of the United States of America*, 112(51), 15743–15748. <http://doi.org/10.1073/pnas.1417059112>
- Kleen, J. K., Testorf, M. E., Roberts, D. W., Scott, R. C., Jobst, B. J., Holmes, G. L., & Lenck-Santini, P.-P. (2016). Oscillation phase locking and late ERP components of intracranial hippocampal recordings correlate to patient performance in a working memory task. *Frontiers in Human Neuroscience*, 10, 1–14. <http://doi.org/10.3389/fnhum.2016.00287>

- Kovach, C. K., Tsuchiya, N., Kawasaki, H., Oya, H., Howard, M. A., & Adolphs, R. (2011). Manifestation of ocular-muscle EMG contamination in human intracranial recordings. *NeuroImage*, 54(1), 213–233. <http://doi.org/10.1016/j.neuroimage.2010.08.002>
- Kramis, R., Vanderwolf, C. H., & Bland, B. H. (1975). Two types of hippocampal rhythmical slow activity in both the rabbit and the rat: Relations to behavior and effects of atropine, diethyl ether, urethane, and pentobarbital. *Experimental Neurology*, 49(1 Pt 1), 58–85.
- Kreiman, G., Koch, C., & Fried, I. (2000). Category-specific visual responses of single neurons in the human medial temporal lobe. *Nature Neuroscience*, 3(9), 946–953. <http://doi.org/10.1038/78868>
- Larsson, L., Nystrom, M., & Stridh, M. (2013). Detection of saccades and postsaccadic oscillations in the presence of smooth pursuit. *IEEE Transactions on Biomedical Engineering*, 60(9), 2484–2493. <http://doi.org/10.1109/TBME.2013.2258918>
- Leonard, T. K., Mikkila, J. M., Eskandar, E. N., Gerrard, J. L., Kaping, D., Patel, S. R., ... Hoffman, K. L. (2015). Sharp wave ripples during visual exploration in the primate hippocampus. *The Journal of Neuroscience*, 35(44), 14771–14782. <http://doi.org/10.1523/JNEUROSCI.0864-15.2015>
- Liebe, S., Hoerzer, G. M., Logothetis, N. K., & Rainer, G. (2012). Theta coupling between V4 and prefrontal cortex predicts visual short-term memory performance. *Nature Neuroscience*, 15(3), 456–462. <http://doi.org/10.1038/nn.3038>
- Lisman, J. E., & Jensen, O. (2013). The theta-gamma neural code. *Neuron*, 77(6), 1002–1016. <http://doi.org/10.1016/j.neuron.2013.03.007>
- Lisman, J. E., & Redish, A. D. (2009). Prediction, sequences and the hippocampus. *Philosophical Transactions of the Royal Society B: Biological Sciences*, 364(1521), 1193–1201. <http://doi.org/10.1098/rstb.2008.0316>
- Liu, Z.-X., Shen, K., Olsen, R. K., & Ryan, J. D. (2017). Visual sampling predicts hippocampal activity. *The Journal of Neuroscience*, 37(3), 599–609. <http://doi.org/10.1523/JNEUROSCI.2610-16.2017>
- Loonis, R. F., Brincat, S. L., Antzoulatos, E. G., & Miller, E. K. (2017). A meta-analysis suggests different neural correlates for implicit and explicit learning. *Neuron*, 96(2), 521–534.e7. <http://doi.org/10.1016/j.neuron.2017.09.032>
- Lund, U. (1999). Least circular distance regression for directional data. *Journal of Applied Statistics*, 26(6), 723–733. <http://doi.org/10.1080/02664769922160>
- McCullagh, P. (2005). Proportional-odds model. In P. Armitage & T. Colton (Eds.), *Encyclopedia of Biostatistics* (pp. 2–4). <http://doi.org/10.1002/0470011815.b2a10049>
- McFarland, J. M., Bondy, A. G., Saunders, R. C., Cumming, B. G., & Butts, D. A. (2015). Saccadic modulation of stimulus processing in primary visual cortex. *Nature Communications*, 6, 1–14. <http://doi.org/10.1038/ncomms9110>
- McKenzie, S., Keene, C., Farovik, A., Blandon, J., Place, R., Komorowski, R., & Eichenbaum, H. (2016). Representation of memories in the cortical-hippocampal system: Results from the application of population similarity analyses. *Neurobiology of Learning and Memory*, 134, 178–191. <http://doi.org/10.1016/j.nlm.2015.12.008>
- McNaughton, B. L., Battaglia, F. P., Jensen, O., Moser, E. I., & Moser, M.-B. (2006). Path integration and the neural basis of the “cognitive map”. *Nature Reviews Neuroscience*, 7(8), 663–678. <http://doi.org/10.1038/nrn1932>
- Meister, M. L. R., & Buffalo, E. A. (2016). Getting directions from the hippocampus: The neural connection between looking and memory. *Neurobiology of Learning and Memory*, 134, 135–144. <http://doi.org/10.1016/j.nlm.2015.12.004>
- Moore, T., Armstrong, K. M., & Fallah, M. (2003). Review: Visuomotor origins of covert spatial attention and oculomotor control mechanisms during scanning eye movements is of particular importance to visual neurobiologists. *Neuron*, 40, 671–683.
- Mormann, F., Fell, J., Axmacher, N., Weber, B., Lehnertz, K., Elger, C. E., & Fernández, G. (2005). Phase/amplitude reset and theta-gamma interaction in the human medial temporal lobe during a continuous word recognition memory task. *Hippocampus*, 15(7), 890–900. <http://doi.org/10.1002/hipo.20117>
- Morris, R. G. M. (2006). Elements of a neurobiological theory of hippocampal function: The role of synaptic plasticity, synaptic tagging and schemas. *European Journal of Neuroscience*, 23(11), 2829–2846. <http://doi.org/10.1111/j.1460-9568.2006.04888.x>
- Muzzio, I. A., Kentros, C., & Kandel, E. (2009). What is remembered? Role of attention on the encoding and retrieval of hippocampal representations. *Journal of Physiology*, 587(12), 2837–2854. <http://doi.org/10.1113/jphysiol.2009.172445>
- Najemnik, J., & Geisler, W. S. (2005). Optimal eye movement strategies in visual search. *Nature*, 19(2004), 387–391.
- Nyström, M., & Holmqvist, K. (2010). An adaptive algorithm for fixation, saccade, and glissade detection in eyetracking data. *Behavior Research Methods*, 42(1), 188–204. <http://doi.org/10.3758/BRM.42.1.188>
- O'Keefe, J., & Recce, M. L. (1993). Phase relationship between hippocampal place units and the EEG theta rhythm. *Hippocampus*, 3(3), 317–330. <http://doi.org/10.1002/hipo.450030307>
- Peelen, M. V., & Kastner, S. (2014). Attention in the real world: Toward understanding its neural basis. *Trends in Cognitive Sciences*, 18(5), 242–250. <http://doi.org/10.1016/j.tics.2014.02.004>
- Place, R., Farovik, A., Brockmann, M., & Eichenbaum, H. (2016). Bidirectional prefrontal-hippocampal interactions support context-guided memory. *Nature Neuroscience*, 19(8), 992–994. <http://doi.org/10.1038/nn.4327>
- Rajkai, C., Lakatos, P., Chen, C. M., Pincze, Z., Karmos, G., & Schroeder, C. E. (2008). Transient cortical excitation at the onset of visual fixation. *Cerebral Cortex*, 18(1), 200–209. <http://doi.org/10.1093/cercor/bhm046>
- Ringo, J. L., Sobotka, S., Diltz, M. D., & Bunce, C. M. (1994). Eye movements modulate activity in hippocampal, parahippocampal, and inferotemporal neurons. *Journal of Neurophysiology*, 71(3), 1285–1288.
- Rizzuto, D. S., Madsen, J. R., Bromfield, E. B., Schulze-Bonhage, A., & Kahana, M. J. (2006). Human neocortical oscillations exhibit theta phase differences between encoding and retrieval. *NeuroImage*, 31(3), 1352–1358. <http://doi.org/10.1016/j.neuroimage.2006.01.009>
- Rolls, E. T. (1999). Spatial view cells and the representation of place in the primate hippocampus. *Hippocampus*, 9(4), 467–480.
- Rolls, E. T., & O'Mara, S. M. (1995). View-responsive neurons in the primate hippocampal complex. *Society for Neuroscience Abstracts*, 19(409), 424.
- Rolls, E. T., Robertson, R. G., & Georges-francois, P. (1997). Spatial view cells in the primate hippocampus. *European Journal of Neuroscience*, 9, 1789–1794.
- Rolls, E. T., & Wirth, S. (2018). Spatial representations in the primate hippocampus, and their functions in memory and navigation. *Progress in Neurobiology*, 171, 90–113.
- Rueckemann, J. W., & Buffalo, E. A. (2017). Spatial responses, immediate experience, and memory in the monkey hippocampus. *Current Opinion in Behavioral Sciences*, 17(1), 155–160. <http://doi.org/10.1016/j.cobeha.2017.08.008>
- Sainsbury, R. S., Harris, J. L., & Rowland, G. L. (1987). Sensitization and hippocampal type 2 theta in the rat. *Physiology and Behavior*, 41(5), 489–493. [http://doi.org/10.1016/0031-9384\(87\)90085-0](http://doi.org/10.1016/0031-9384(87)90085-0)
- Samonds, J. M., Geisler, W. S., & Priebe, N. J. (2018). Natural image and receptive field statistics predict saccade sizes. *Nature Neuroscience*, 2, 1591–1599. <http://doi.org/10.1038/s41593-018-0255-5>
- Sarma, Y., & Jammalamadaka, S. R. (1993). Circular regression. In K. Matusita, M. L. Puri, & T. Hayakawa (Eds.), *Proceedings of the Third Pacific Area Statistical Conference: Statistical sciences and data analysis* (pp. 109–128). Utrecht, The Netherlands: VSP.
- Schiller, D., Eichenbaum, H., Buffalo, E. A., Davachi, L., Foster, D. J., Leutgeb, S., & Ranganath, C. (2015). Memory and space: Towards an understanding of the cognitive map. *Journal of Neuroscience*, 35(41), 13904–13911. <http://doi.org/10.1523/JNEUROSCI.2618-15.2015>

- Schroeder, C. E., & Lakatos, P. (2009). Low-frequency neuronal oscillations as instruments of sensory selection. *Trends in Neurosciences*, 32(1), 9–18. <http://doi.org/10.1016/j.tins.2008.09.012>
- Schroeder, C. E., Wilson, D. A., Radman, T., Scharfman, H., & Lakatos, P. (2010). Dynamics of active sensing and perceptual selection. *Current Opinion in Neurobiology*, 20(2), 172–176. <http://doi.org/10.1016/j.conb.2010.02.010>
- Skaggs, W. E., McNaughton, B. L., Permenter, M., Archibeque, M., Vogt, J., Amaral, D. G., & Barnes, C. a. (2007). EEG sharp waves and sparse ensemble unit activity in the macaque hippocampus. *Journal of Neurophysiology*, 98(2), 898–910. <http://doi.org/10.1152/jn.00401.2007>
- Sobotka, S., Nowicka, A., & Ringo, J. L. (1997). Activity linked to externally cued saccades in single units recorded from hippocampal, parahippocampal, and inferotemporal areas of macaques. *Journal of Neurophysiology*, 78(4), 2156–2163.
- Sobotka, S., & Ringo, J. L. (1997). Saccadic eye movements, even in darkness, generate event-related potentials recorded in medial septum and medial temporal cortex. *Brain Research*, 756(1–2), 168–173. [http://doi.org/10.1016/S0006-8993\(97\)00145-5](http://doi.org/10.1016/S0006-8993(97)00145-5)
- Sommer, M. A., & Wurtz, R. H. (2002). A pathway in primate brain for internal monitoring of movements. *Science*, 296(5572), 1480–1482. <http://doi.org/10.1126/science.1069590>
- Sommer, M. A., & Wurtz, R. H. (2006). Influence of the thalamus on spatial visual processing in frontal cortex. *Nature*, 444(7117), 374–377. <http://doi.org/10.1038/nature05279>
- Staudigl, T., Hartl, E., Noachtar, S., Doeller, C. F., & Jensen, O. (2017). Saccades are phase-locked to alpha oscillations in the occipital and medial temporal lobe during successful memory encoding. *PLoS Biology*, 15(12), e2003404. <http://doi.org/10.1371/journal.pbio.2003404>
- Tallon-Baudry, C., Bertrand, O., Delpuech, C., & Pernier, J. (1997). Oscillatory gamma-band (30–70 Hz) activity induced by a visual search task in humans. *The Journal of Neuroscience: The Official Journal of the Society for Neuroscience*, 17(2), 722–734. <http://doi.org/10.1007/s11064-011-0538-7>
- Tesche, C. D., & Karhu, J. (2000). Theta oscillations index human hippocampal activation during a working memory task. *Proceedings of the National Academy of Sciences*, 97(2), 919–924. <http://doi.org/10.1073/pnas.97.2.919>
- Thompson, K. G., Hanes, D. P., Bichot, N. P., & Schall, J. D. (1996). Perceptual and motor processing stages identified in the activity of macaque frontal eye field neurons during visual search. *Journal of Neurophysiology*, 76(6), 4040–4055.
- Tremblay, S., Doucet, G., Pieper, F., Sachs, A., & Martinez-Trujillo, J. (2015). Single-trial decoding of visual attention from local field potentials in the primate lateral prefrontal cortex is frequency-dependent. *Journal of Neuroscience*, 35(24), 9038–9049. <http://doi.org/10.1523/JNEUROSCI.1041-15.2015>
- Vass, L. K., Copara, M. S., Seyal, M., Shahlaie, K., Farias, S. T., Shen, P. Y., & Ekstrom, A. D. (2016). Oscillations go the distance: Low-frequency human hippocampal oscillations code spatial distance in the absence of sensory cues during teleportation. *Neuron*, 89, 1–7. <http://doi.org/10.1016/j.neuron.2016.01.045>
- Watrous, A. J., & Ekstrom, A. D. (2014). The spectro-contextual encoding and retrieval theory of episodic memory. *Frontiers in Human Neuroscience*, 8, 1–15. <http://doi.org/10.3389/fnhum.2014.00075>
- Watrous, A. J., Fried, I., & Ekstrom, A. D. (2011). Behavioral correlates of human hippocampal delta and theta oscillations during navigation. *Journal of Neurophysiology*, 105(4), 1747–1755. <http://doi.org/10.1152/jn.00921.2010>
- Wirth, S., Baraduc, P., Plante, A., Pinede, S., Duhamel, J.-R. (2017). Gaze-informed, task-situated representation of space in primate hippocampus during virtual navigation. *PLoS Biology*, 15(2), 1–28. <http://doi.org/10.1371/journal.pbio.2001045>
- Zanos, S., Zanos, T. P., Marmarelis, V. Z., Ojemann, G. a., & Fetzi, E. E. (2012). Relationships between spike-free local field potentials and spike timing in human temporal cortex. *Journal of Neurophysiology*, 107(7), 1808–1821. <http://doi.org/10.1152/jn.00663.2011>
- Zanos, T. P., Mineault, P. J., & Pack, C. C. (2011). Removal of spurious correlations between spikes and local field potentials. *Journal of Neurophysiology*, 105(1), 474–486. <http://doi.org/10.1152/jn.00642.2010>
- Zimmermann, E., & Lappe, M. (2016). Visual space constructed by saccade motor maps. *Frontiers in Human Neuroscience*, 10(May), 225. <http://doi.org/10.3389/fnhum.2016.00225>

SUPPORTING INFORMATION

Additional supporting information may be found online in the Supporting Information section at the end of this article.

How to cite this article: Doucet G, Gulli RA, Corrigan BW, Duong LR, Martinez-Trujillo JC. Modulation of local field potentials and neuronal activity in primate hippocampus during saccades. *Hippocampus*. 2020;30:192–209. <https://doi.org/10.1002/hipo.23140>